WAGENINGEN
UNIVERSITY & RESEARCH

The effect of including leaf optical and photosynthetic vertical profiles on the functionality of the Digital Tomato Crop

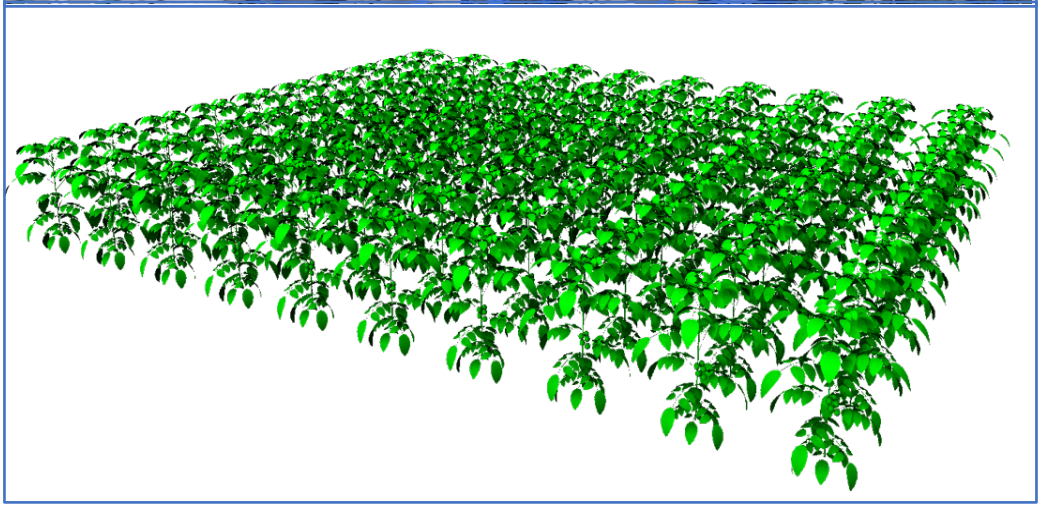

Name Student: *Rutger Vreezen*

Student ID: *1034952*

Course Code: *HPP-80436*

Completion Date: *3rd of June 2022*

Supervisors: *Dr. N (Nastassia) Vilfan & Dr. K (Katarina) Streit*

Table of Contents

1. Abstract

Wageningen Research is building a digital twin of a greenhouse crop called the "Virtual Tomato Crops" (VTC). The VTC is based on the concepts of functional-structural plant (FSP) modelling. Commonly, all leaves within the crop are represented by identical optical and photosynthetic parameters. However, literature showed that mid-canopies of trees had lower leaf light absorption and higher light transmittance compared to the upper canopy. Furthermore, it has been shown that the photosynthetic capacity progressively decreases downwards within the crop. The research aim of this study was to assess the value of adding vertical crop complexity by including distinct leaf optical and photosynthetic parameters for the higher and lower leaf layer within the FSP model. A greenhouse experiment was set up including three tomato varieties (Brioso, Merlice, Moneymaker). The measurements were used to parametrize the FSP model. The measurements for the Merlice variety showed a 2.9 % higher light absorption, 28.9% lower light transmittance and a 32% lower photosynthetic capacity of the lower leaf layer compared to higher leaf layer. By including the vertical gradient for leaf optical properties in the model, the simulations showed an increase in crop light interception (9.0%), photosynthesis (8.9%), and growth (8.9%). While, by including the vertical photosynthesis gradient, crop light interception (27.6%), photosynthesis (30.1%), and growth (29.9%) were effectively decreased. It was concluded that the leaf optical and photosynthetic parameters had a substantial effect on the VTC model predictions, and the vertical profiles should for that reason be considered in FSP model simulations.

2. Introduction

2.1 Digital Twin

Crop models have been used in horticulture for growth predictions and scientific analysis of eco-physiological processes for decades (Marcelis *et al*., 1998). Wageningen Research has set up the digital twin project called the "Virtual Tomato Crops" (VTC) that aims at developing a 3D tomato growth simulation model. The VTC experiment was conducted at NPEC (Netherlands Plant Eco-phenotyping Centre). NPEC is a joint initiative of Wageningen University & Research and Utrecht University and facilitates high-through put phenotyping and high-resolution data from plants above and below ground (NPEC, 2022). By using the data from a set-up of climate and plant sensors, the tomato model will be continuously updated, thereby generating a real-time virtual counterpart of the tomato plants within the NPEC greenhouse. The aim of the VTC development is to better understand the underlying concepts of crop and greenhouse simulation. With the improved insights an increase in greenhouse resource use efficiency can be realised regarding (artificial) lighting, CO_2 supplementation, greenhouse heating, and substrate watering. Moreover, stakeholders of the VTC (e.g. growers, breeders, suppliers and consultants) can use the output of the VTC to improve greenhouse climate settings, pruning strategies, testing greenhouse covers, and selecting superior crop traits (Figure 1).

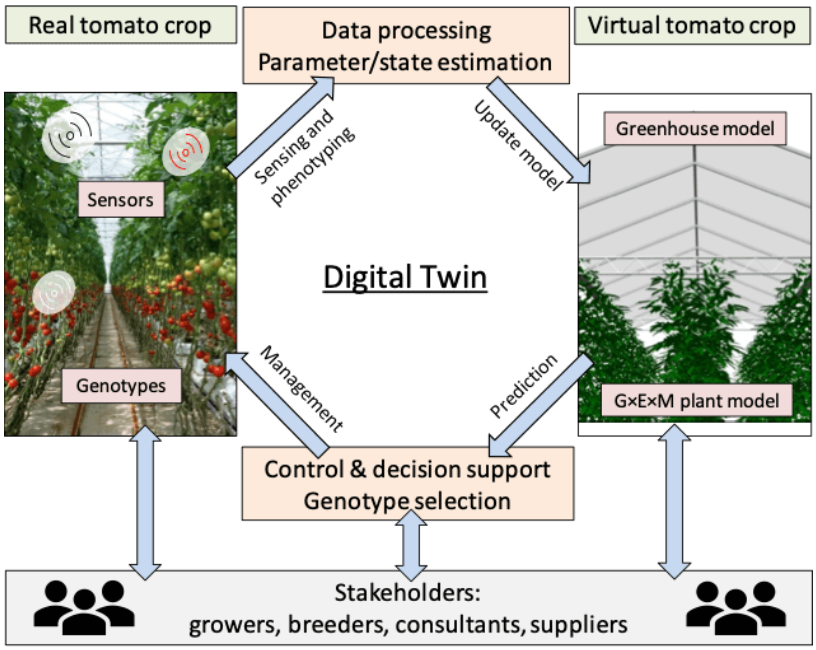

Figure 1. Schematic relationship diagram of the VTC including the real and virtual tomato crop and the underlying processes of sensing, phenotyping, data processing, model updating, model predictions, decision support, and crop management (NPEC, 2022).

2.2 Functional-structural plant models

The greenhouse crop simulation of the VTC is based on the concepts of FSP (functional-structural plant) modelling (NPEC, 2022). FSP modelling deals with the crop performance in respect to phenotypic plasticity, plant to plant interaction, plant architecture, and canopy and environmental heterogeneity (Godin & Sinoquet, 2004; Evers *et al.*, 2010; Evers *et al.*, 2018; Vos *et al.*, 2010). FSP models simulate in three-dimensions the continuous feedback between environmental drivers, plant functioning and structure (Vos *et al.*, 2010). These models treat the plants as a collection of individual organs and simulate their interaction with the local climate (Muller *et al.*, 2007). Typical FSP models at crop level contain three major components including growth, development, and architecture. The growth and development in FSP models are driven by light interception and temperature. Interception of light within the canopy is determined by the incoming light and the distribution of leaf area within the canopy. The assimilation of CO_2 (carbon dioxide) by photosynthesis is driven by the light absorption and is dependent on leaf nitrogen content, stomatal conductance, air temperature, and CO_2 concentration. The organ growth rate is dependent on the amount of assimilates, respiration rate, the source / sink ratio, and developmental stage. In each model loop the three-dimensional placement of every individual leaf, internode and other relevant organ is updated. With the updated plant architecture, the light interception is calculated again and thereby closing the loop (Evers & Marcelis, 2019) (Figure 2).

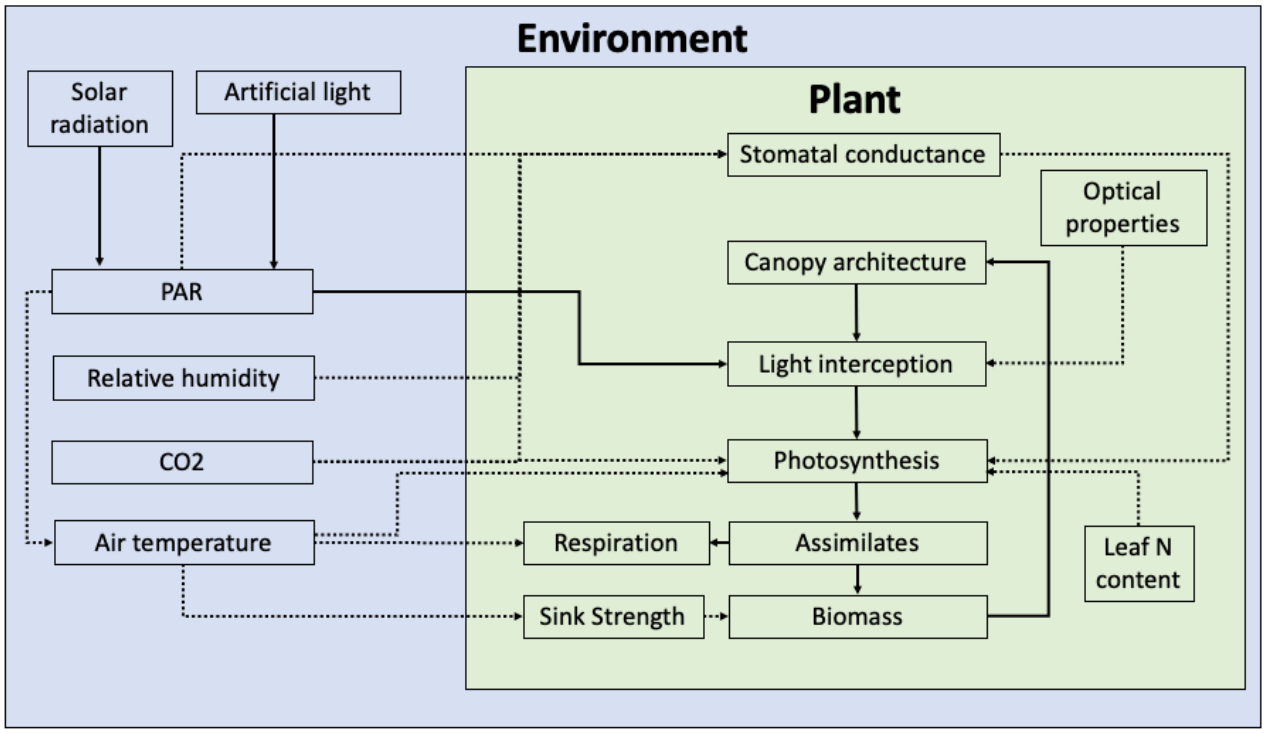

Figure 2. Schematic relationship diagram of a Functional-Structural Plant model including unbroken arrows (→) representing the flow of physical quantities (e.g. PAR, assimilates) and interrupted arrows (⇢) that indicate the variable had influence on another variable (e.g. the effect of optical properties on the light interception).

2.3 Model of light interception

Light models simulate the radiative fluxes that each organ receives by estimating the radiative exchange between the light source and the organs. Multiple light simulation models can be used to represent the direct and diffuse sunlight or supplementary lighting above the canopy. For field conditions, typically a dome of light sources is used to represent direct or diffuse light coming from the sky. An arc of light sources at different heights is used to represent the course of the sun during the day (Figure 3) (Chelle & Andrieu, 2007; Evers *et al.*, 2010). The intensity of light sources can be determined by actual weather data or mathematic models' approximations (Goudriaan & Van Laar, 2012). Phylloclimate modelling is used to calculate the amount of radiation that reaches each individual photosynthetic organ. Ray tracing is one of the methods that simulates the path and the interaction of photons with the leaves of the canopy until the photons either are absorbed or exit the canopy. The light can be simulated both through the source-based (ray traced from light source to canopy) or recipient-based approach (ray traced from organs to the light source) (Chelle & Andrieu, 2007). The intensity of the incoming light is dependent on the light source and the three-dimensional orientation between the

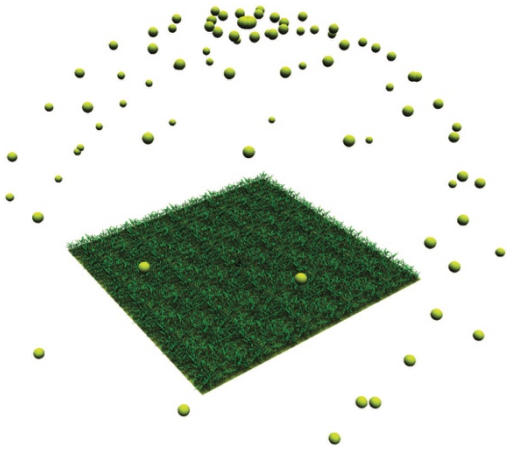

Figure 3. Field of simulated maize plants showing the dome and arc of light sources that emit the radiation. (Evers & Marcelis, 2019).

light source and the plant organ (Evers & Marcelis, 2019). The amount of radiation absorbed by a leaf is determined by the amount of incoming Photosynthetically Active Radiation (PAR), the leaf orientation and positioning, and leaf optical properties (absorption, reflectance, transmittance). By use of the transmittance and reflectance of the leaves the light absorption distribution within the canopy is calculated (Cieslak *et al.*, 2008; Hemmerling *et al.*, 2008).

2.4 Carbon assimilation & Organ sink strength

The immediate leaf photosynthesis is dependent on the local climate conditions of absorbed light, CO_2, and temperature. Moreover, the leaf photosynthesis can through the process of acclimation change over time. The non-rectangular hyperbola (NRH) from Thornley can be used to calculate the leaf photosynthesis. (A_{leaf}[$\mu mol\ CO_2\ m^{-2}\ s^{-1}$]). The NRH is determined by: the independent variable of the upper leaf surface photon flux (I_{Leaf} [$\mu mol\ m^{-2}\ s^{-1}$]) and three parameters: the apparent quantum yield (α [$mol\ CO_2\ photon^{-1}$], NRH curve convexity (ξ [$dimensionles$]) and the light saturated value of photosynthesis (A_{sat} [$\mu mol\ CO_2\ m^{-2}\ s^{-1}$]). By subtracting the leaf dark respiration rate (R_{d} [$\mu mol\ CO_2\ m^{-2}\ s^{-1}$]) the net photosynthesis can be calculated by the model (Equation 1).

$$A_{leaf}\ (I_{Leaf}) = \frac{\alpha I_{Leaf} + A_{sat} - \sqrt{[(\alpha I_{Leaf} + A_{sat})^2 - 4\xi\alpha\ I_{Leaf} A_{sat}\ ]}}{2\xi} - R_d$$

Equation 1. The formula for the non-rectangular hyperbola (NRH) from Thornley including the incident photon flux (I_{Leaf} [$\mu mol\ m^{-2}\ s^{-1}$]), apparent quantum yield (α [$mol\ CO_2\ photon^{-1}$], NRH curve convexity (ξ [$-$]), light saturated value of photosynthesis (A_{sat} [$\mu mol\ CO_2\ m^{-2}\ s^{-1}$]).

Using the NRH approach, the total amount of assimilates per photosynthetic organ can be determined (Thornley, 1998). For small annual crop species with model time steps of one day it is assumed that all assimilates can potentially reach any organ within the plant. The allocation of the assimilates pool for organ growth is simulated based on sink strength and the balance between the supply and demand of assimilates (Allen *et al.*, 2005; Bongers *et al.*, 2018). The organ sink strength, assimilates availability and the between organ competition for assimilates continuously changes over time. Therefore, the assimilate allocation is calculated every time step.

2.5 VTC model improvement

Simulation modelling is about finding the balance between what to include and what to leave out depending on the research question. For FSP models the "tailored" modelling principle is used where complexity of the model is matched with the research questions. The incorporation of additional model mechanisms can decrease the computational efficiency, increase parameter requirement, and may induce additional variation (Evers & Marcelis, 2019). FSP models use the individual leaf light levels to calculate the light absorption and photosynthesis rates. In most FSP models to scale up the functioning of a photosynthetic organs to the crop level all leaves are assumed to have the identical leaf optical and photosynthetic parameters. Often the most

recently matured top leaf in a growing plant is used to represent all leaves of the crop. This simplification could compromise on the accuracy of the model calculations of the crop light interception and photosynthesis. Namely, Trouwborst *et al*. (2011) showed that leaf photosynthetic capacity progressively decreases as result of the shading effect of new grown leaves. As a consequence, it was found that the leaves in the lower leaf layer had a lower photosynthetic capacity compared to higher canopy leaves due to the low light acclimation. For tomato crop species little research is available on the optical properties over a vertical gradient. However, it has been shown in forest canopies that one-layer homogeneous canopy reflectance models can impose a systematic error in estimating the directional reflectance (Kuusk, 2001). In addition, it has been shown in some tropical rainforest trees species that the mid-canopy leaves had higher absorption compared to the higher canopy leaves. Also it was shown that the mid-canopy and understory leaves had a lower light transmittance compared to the higher canopy leaves (Poorter *et al*., 1995). Furthermore, it has been shown that for cucumber and spinach the unshaded lower leaf layer showed higher chlorophyl a and b concentrations compared to the shaded middle and lower leaf layer. The higher leaf chlorophyl concentrations also suggest higher leaf light absorption (Cui *et al*., 1991; Kaiser *et al*., 2019). The aim of this research is to analyse the effect of canopy heterogeneity in the simulated virtual tomato crop for the temporary dynamics of the crop vertical light distribution, light interception, and photosynthesis. Based on the research aim two research questions and hypothesis have been formulated:

Research questions

1. What is the effect of including unique parameters for leaf optical properties (transmittance and reflectance) for the higher and lower leaf layer on the total crop light absorption, photosynthesis, growth, and yield FSP model prediction?
2. What is the effect of including unique parameters of leaf photosynthesis (α, ξ and A_{max}) for the higher and lower leaf layer on the total crop photosynthesis, growth, and yield FSP model prediction?

Research hypotheses

1. Including unique parameters for leaf optical properties (transmittance and reflectance) for the higher and lower leaf layer will increase the total crop light interception due to the higher average light absorption and lower light transmittance of the lower canopy leaves. Due to the higher crop light interception also crop photosynthesis, growth and yield prediction will be higher.
2. Including unique parameters of leaf photosynthesis (α, ξ and P_{max}) for the higher and lower leaf layer will decrease crop photosynthesis rate. Since the photosynthetic rate of the lower leaves is lower due to the low light acclimation of the leaves the overall crop photosynthesis is reduced. Therefore, including a photosynthesis profiles will decrease the growth and yield predictions by the FSP model.

3. Material & Methods

3.1 Cultivation practices

A pot experiment was carried out in the NPEC greenhouse in compartment 1 (12 × 12 m dimensions) at Wageningen University & Research (52°N, 6°E, Wageningen, the Netherlands). The tomato plants (*Solanum lycopersicum*) were placed in single carries and moved through the compartments by use of conveyor belts (Figure 4). Each plant was supported by a stick to facilitate the controlled vertical growth. Three different tomato cultivars were used for the experiment: Merlice, Moneymaker and Brioso. All three cultivars had an indeterminate growth type. Before the experiments all seeds were sown in germination soil the 9 / 9 / 2021 at the Unifarm greenhouse in Wageningen. On the 24 / 9 / 2021 the plants were transplanted into 23 cm diameter pots that were filled with quartz sandy soil. On the 27 / 9 / 2021 (0 Days After Start) the plants were relocated to the NPEC greenhouse until the end of the experiment the 30 / 11 / 2021 (64 DAS). To determine the maximum organ dimension the plants were decapitated the 3 / 12 / 2021 and grown until the 20 / 12 / 2021. During the whole experiment the side shoots were pruned weekly. The flowers (i.e. when the fruit was set) were pruned weekly. Brioso was pruned to remain 10 flowers and Moneymaker and Merlice were pruned until 5 flowers remained. The plants were irrigated with a nutrient solution containing 1.20 mM NH_4^+, 7.20 mM K^+, 4.09 mM Ca^{2+}, 1.82 mM Mg^{2+}, 12.42 mM NO_3^-, 3.34 mM SO_4^{2-} , 1.14 mM PO_4^{3-}, 25.00 µM Fe^{3+}, 10.00 µM Mn^{2+} , 5.00 µM Zn^{2+}, 30.00 µM BO_3^{3-}, 0.75 µM Cu^{2+} and 0.5 µM MoO_4^{2-}. The Electrical Conductivity (EC) was set to 2.0 mS/cm. All pots were watered every night (between 22:00-05:00h) by use of a precision weight measurement. Due to technical errors three nights (26/10/2021, 7/11/2021, and 24/11/2021) occurred in which the plants received delayed water in the afternoon. This could have compromised the plant growth and development.

Figure 4. Showing the tomato plants in single carrier conveyer belts placed in the 23 cm pots with the growth sticks.

3.2 Greenhouse climate control

A Hoogendoorn climate computer regulated the climate in the compartment. The greenhouse day / night temperature was set to 22 / 18ºC and air humidity to 70%. The temperature was controlled by a heating and cooling system. In addition, the air humidity was controlled through a dehumidification installation and a nozzle misting system. CO_2 fertilization was applied and set at 700 ppm, however the supplementation was only effective after the 1 / 11 / 2021 (35 DAS). The compartment was equipped with a LED lighting system (VYPR $2x^2$; Fluence; USA) and the plants were effectively exposed to 16 hours of light per day. The natural sunset determined at what time 8 hours later the lights were switched on. A light reflecting screen was used when the lights were switched on during the night to avoid light pollution. The LED lighting was switched on when the measured outside radiation was lower than 150 W m^{-2}. The LED Lighting was switched off when the

184 outside radiation was higher than 250 W m^{-2}. The LED lights provided on average a photosynthetic photon
185 flux density (PPFD) of ±150 μmol m^{-2} s^{-1} at top canopy level when the plants were 1.5 m tall. The energy
186 screen and solar screen were not used during the experiment. The blackout screen was used when the lights
187 were turned on at night to avoid light pollution.
188
189 ## 3.3 Experimental design
190 The experiment consisted of 282 plants distributed over 35 rows and 16 columns (Figure 5). The plants were
191 moved through conveyor belts in the direction of the columns for the daily overnight watering and 3D scanning
192 3 times per week. All three varieties had three to six replicates reserved for the destructive harvest (between
193 week 1 to week 8). The harvested plants were replaced with border plants to maintain the canopy. A resolvable
194 row-column design was generated including four subblocks. Outside the blocks the replacement plants were
195 positioned within the greenhouse. Within each block the three cultivars were randomly allocated to a spot.
196 However, within each block a restricted maximum was enforced of each cultivar per rows and columns.
197 Thereby evenly distributing all three cultivars throughout the experimental layout. In total all four blocks
198 contained 126 experimental plants over a 52.5 m^2 surface area (0.42 m^2 $plants^{-1}$).

Figure 5. Resolvable row column experimental design (4 blocks) including 35 rows (1 – 35) and 16 columns (AA – AP). In total 282 plants divided over 3 cultivars (Brioso, Merlice, Money Maker).

3.4 Experimental measurements

3.4.1 PAR, temperature, and CO2 measurements

For the temperature measurements, 1 Hoogendoorn aspirator box (Hoogendoorn-Economic; Hoogendoorn; The Netherlands) and 9 Sigrow sensors (Air+; Sigrow; The Netherlands) were used. Moreover, the Sigrow sensors and WUR-made PAR bars measured Photosynthetic Photon Flux Density (PPFD) and the Hoogendoorn aspirator box measured the CO_2 concentration. Based on the average daily PPFD and the daylength the Daily Light Integral (DLI) was calculated. Nine wooden sticks were evenly spatially distributed with on top a Sigrow sensors. The PAR bars measured PAR at 5 locations above the tomato crop (Figure 6). Unfortunately, since the PAR bars were not rightly calibrated the data of the PAR bars was not used in this study.

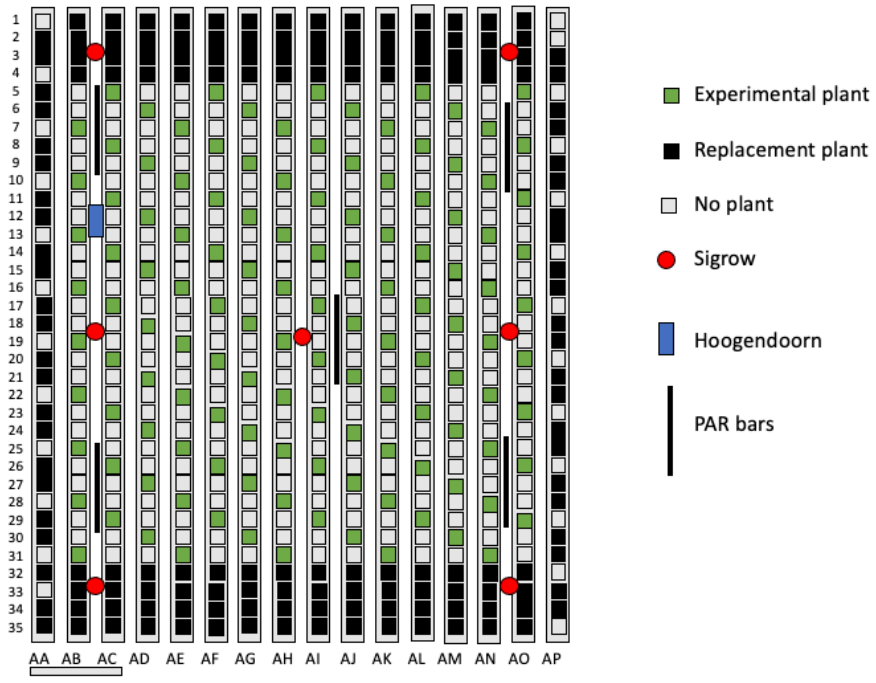

Figure 6. Sensor location throughout the experimental layout including the experimental plants (green) and the replacement plants (black). The Sigrow sensors (red), PAR bars (black) and Hoogendoorn aspirator box (blue).

3.4.2 Leaf optical properties

Leaf reflectance and transmittance were measured with two spectrometers (STS-VIS miniature Spectrometer; Ocean Optics; Germany) as shown in Figure 7A & 7C. All leaflets were cut of the plant in the morning, placed in plastic sheets and stored in a cold room to minimize any transpirational water loss. Each plastic sheet was labelled with the location and cultivar name (Figure 7B). Spectrometer calibration was conducted after every 8 leaflet measurements. In week 5 the first measurements were conducted on 42 DAS (8/11/21) and week 7 the second measurements were conducted on 56 DAS (22/11/21) (Figure 9). In total, 54 measurements were conducted for the first measuring day (3 cultivars × 3 replicates × 1 leaf (one leaf layers) × 3 leaflets per leaf × 2 leaflet sides (adaxial & abaxial)). In total, 72 measurements were conducted for the second measuring day (3 cultivars × 3 replicates × 2 leaves (two leaf layers) × 2 leaflets per leaf × 2 leaflet sides (adaxial & abaxial)). The first leaf below the first truss was measured the first measuring day (one leaf layer). The second measuring day the leaf below the first truss and first leaf below the second truss were measured (two leaf layer). During this experiment all phytomer ranks were counted from the bottom to top. The optical properties higher leaf layer was determined as all measurements conducted on 42 DAS (8/11/21) and the measurements conducted on 56 DAS (22/11/21) of phytomer ranks above 10. The lower leaf layer was determined as measurements conducted on 56 DAS (22/11/21) of phytomer ranks below or including 10. The spectrometer protocol was written by ing. Peter van der Putten and can be provided on request. It was found that the light source of the two spectrometers that were used, were malfunctioning for the measurements in the region of 400 – 450 nm. For that reason, only the absorption, reflectance, and transmittance of the 450 – 700 nm region were considered in the FSP modelling.

Figure 7. The two spectrometers (A), the leaflets as stored in plastic sheets (B) and the measurement software (C).

3.4.3 Photosynthesis

A portable photosynthesis system (Li-6800; LI-COR Biosciences; USA) was used starting 38 DAS (1/11/21) for four consecutive weeks. The measurements were conducted between 9:00h – 16:00h in the neighbouring compartment 3, with identical climate settings as in compartment 1. A chamber aperture of 2 cm^2 was used for all Li-6800 measurements. The flow rate was set to 10,000 $\mu mol\ s^{-1}$, the relative humidity to 60%, the light to 10% blue and 90% red light and leaf temperature at 25 ºC. The Li-6800 program conducted a LRC (Light Response Curve) and A/Ci curves (net CO_2 assimilation rate, A, versus calculated intercellular CO_2, Ci), written by Dr. M.E. (Elias) Kaiser and S.R. (Sarah) Berman. Intercellular CO_2 (Ci) was chosen to minimize any influence of the stomata, mesophyll, and boundary layer conductance. The leaves were acclimated to 400 ppm ambient CO_2 with 400 $\mu mol\ m^{-2}\ s^{-1}$ PPFD and after 2000 $\mu mol\ m^{-2}\ s^{-1}$ PPFD for both a maximum of 20 minutes. Afterwards, a LRC was conducted with time steps of a maximum of 2 minutes and including the following levels of PPFD: 1500, 1000, 800, 600, 400, 200, 150, 100, 50, 0 $\mu mol\ m^{-2}\ s^{-1}$. Next, the leaf was acclimated at 1500 $\mu mol\ m^{-2}\ s^{-1}$ PPFD for 5 – 20 minutes. Finally, The A/Ci curve was started that included 2 – 5 minutes time steps of: 300, 200, 100, 50 ppm ambient CO_2. Subsequently, the leaf was again acclimating at 400 ppm CO_2 for 5 – 20 minutes and thereafter consecutive 600, 900, 1200, 1500, 1800 ppm CO_2. During each step the Li-6800 logged the data. The full program took between 70 – 100 minutes per leaf. The first leaf below the first truss was measured week 4 and week 5 (1 leaf layer). Week 6 and week 7 the second leaf below the first truss and first leaf below the second truss was measured (two leaf layers). In case the leaf was senescent or damaged then a one rank lower leaf in the canopy was chosen. The higher leaf layer for the photosynthesis measurements was determined as all measurements conducted in the 4^{th} and 5^{th} week and the measurements conducted in the 6^{th} and 7^{th} that were of phytomer rank above 10. The lower leaf layer was determined as all measurements of the 6^{th} and 7^{th} week that were of phytomer ranks below or including 10 (Figure 8). During this experiment all phytomer ranks were counted from the bottom to top. Every morning before the measurements the drierite and CO_2 ampul were replaced and demineralized water was added to the humidifier. The soda lime was replaced at the start of every week. The maximum chamber CO_2 concentration was recorded and any warnings that occurred during warm-up tests. After the leaf was clamped to the chamber, a photo of the plant was taken. Furthermore, the chamber was checked for air leaks and if the initial leaf photosynthesis rate was above 5.0 $\mu mol\ m^{-2}\ s^{-1}$ and stomata conductance above 0.10 $mol\ m^{-2}\ s^{-1}$. In case the photosynthesis rate or stomata conductance were lower than the above thresholds another leaflet was chosen.

293

Figure 8. Li-6800 measurements of the higher leaf layer (left) and lower leaf layer (right) in compartment 3.

3.4.4 Destructive harvest

The destructive harvesting was conducted on a weekly basis for eight weeks. The first destructive harvest started the 12 / 10 / 2021 (15 DAS). The first two weeks of the experiment 9 plants (3 varieties and 3 replicates) were harvested and from the third week onwards 18 plants per week were harvested (3 varieties and 6 replicates) (Figure 9). The plants were cut off at the base and the fresh weight, dry weight and leaf area measurements were both measured at the plant and organ level (see Appendix A). The weight measurements were conducted with a precision scale and leaf area with a leaf area meter (LI-3100; LI-COR Biosciences; USA). All plant samples were dried in ovens at 70 ºC for at least 72 hours at Agros, Unifarm. During the 7th and 8th destructive harvest, the plants became considerable large. During the 7th and 8th harvest at plant level leaf area samples were taken between the 1st and 3rd truss. Moreover, at organ level the plants were only harvested above the 5th rank for the leaf dry weight and leaf area measurements. Furthermore, the sample size was decreased for the measurements of the internode fresh weight. Thereby, reducing the harvesting workload. For that reason, the stem dry weight, leaf dry weight, and leaf area were underestimated. Moreover, the lower leaves of Moneymaker were accidently cut during the automatic watering. This caused Moneymaker to have a lower leaf area and leaf dry weight during the whole experiment. The Leaf Area Index (LAI) was calculated as the leaf area per plant divided by the average ground surface area per plant (0.42 m^2 $plants^{-1}$).

3.4.5 Timeline

The experimental timeline including all the measurements (figure 9).

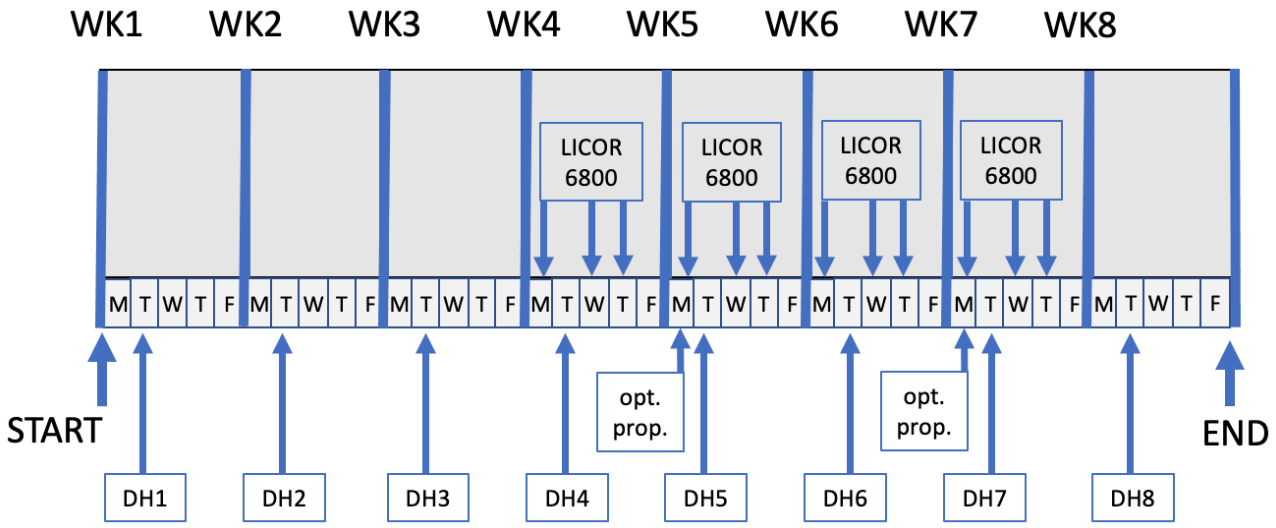

Figure 9. Schematic overview of the experimental measurements from week 1 (WK1) to week 8 (WK8). The figure shows the weekly destructive harvest (DH), two optical properties measuring days (opt. prop.) and photosynthesis measurements (Licor6800). The PPFD, air temperature, CO_2 and relative humidity measurements were conducted throughout the whole experiment by the Hoogendoorn aspirator box, 9 Sigrow sensors, and 5 PAR bars.

3.5 Statistical analysis

An one-way ANOVA was conducted to test the significant effect of the factor "leaf layer" (higher and lower leaf layer) for the response variables leaf absorption, reflectance, transmittance, net photosynthesis rate and stomata conductance. The Tukey's HSD (Honestly Significant Difference) was used to test the significant effect of the factor "Cultivar" (Brioso, Merlice, and Moneymaker) for the response variables leaf absorption, reflectance, transmittance, photosynthesis, stomata conductance, and dry weight measurements (leaves, stems, and trusses) of the 6th harvest. Each response variable was tested for normality with the Shapiro-Wilk test and tested for homogeneity of variances with the Bartlett's test. LOG transformation was carried out if the normality or homogeneity assumption were not meet. The mean differences were considered statistically significant at $P \leq 0.05$. The statistical analyses were performed by use of the open-source software program Python 3 (version 2.7) using multiple libraries (see Appendix B). All statistical output was provided in the supplementary materials (see Appendix B).

3.6 Model Simulations

3.6.1 Model description

The simulations were performed in GroIMP (Growth Grammar-related Interactive Modelling Platform), version 1.6. The download link can be found in the reference (*Index of/GroIMP*, 2011). The software contains features including interactive editing of scenes, an extensive set of 3D objects including colours and textures. Moreover, it uses real-time rendering and the built-in raytracer Twilight. This software mainly distinguishes itself by the modelling potential of relational growth grammars (RGGs). Relational growth grammars is a rule-based approach to the modelling of dynamic systems (Kurth *et al*., 2004). Relational growth grammars are an extended variant of L–systems based on the concepts of graph rewriting. The grammars make it feasible to simulate far-reaching interactions (e.g. overshadowing of plant leaves) (Department Ecoinformatics, 2011). The model was implemented in the language XL (eXtended L-systems), which extends Java by implementation of the RGG formalism. The original FSP tomato model was partially calibrated for the Merlice variety by use of the photosynthesis, leaf optical properties, destructive and climate measurements. The growth module was not fully finished during this study, however sufficiently calibrated to find differences for the different scenarios. In case of the climate measurements the daily averages of temperature, relative humidity, and CO_2 were used as model inputs. The functional-structural plant model consists of several distinct modules (Figure 10):

- **The Light module**: The light was simulated through the source-based ray tracing (from light source to canopy) as described by Hemmerling *et al*. (2008). This model used reflectance and transmittance parameters of the adaxial and abaxial side of the leaf to calculate the leaf absorption with the Twilight model. Diffuse light was modelled using 72 light sources representing a sky dome. Direct light was modelled using an arc of 24 light sources representing the sun positions during the day. Unfortunately, in the experiment accurate light measurements were lacking. Therefore, the model of Goudriaan & Van Laar (2012) was used to simulate the sun and sky intensity. Moreover, a model condition was made that if the PPFD was below 150 μmol m^2 s^{-1} at crop level then it was set to 150 μmol m^2 s^{-1}. These simplifications affected greatly the simulated growth. Plant cloning was used to eliminate the border effect of the simulated plant. The light absorption was calculated based on a focal plant that was cloned in x and y direction. Thereby, the light absorbed by the focal plant is the average of all its clones. All other processes regarding organ development, photosynthesis, and partitioning were only calculated on the focal plant. During this study only one focal plant was used in the simulation. The current model version did not support a small crop patch yet (e.g. 5x5 focal plants).
- **Photosynthesis module:** By use of linear optimisation, the three parameters for the non-rectangular hyperbola including α (apparent quantum yield), ξ (curve convexity) and A_{sat} (light-saturated photosynthesis rate) were fitted to the averages LRC for each tomato variety. The respiration was calculated as a constant fraction of the amount of assimilates. For that reason, leaf respiration was not determined in the linear optimization by using the the 'scipy' python library (see Appendix B).

- **The architectural module**: This dynamic model simulates the plant structure in space and topology of the plant organs using eXtended L-systems as described by Hemmerling *et al*. (2008). This module described the dynamic individual organ shape (e.g. area, length, width) and orientation (e.g. leaf angle) as determined by the destructive harvesting measurements.
- **The development module:** This dynamic model simulates the creation and development of new organs of the virtual plants.
- **The growth module:** This dynamic model determines the growth rate of an organ based on the sink-source balance of the virtual plants. During the simulations the conversion of biomass into the organ dimension was set as a constant value independent of the organ age and rank (specific leaf area [m^2/g] and specific internode length [mm/mg]) . However, data suggests that the conversion of biomass into organ dimensions is dynamic. These simplifications affected greatly the simulated growth.

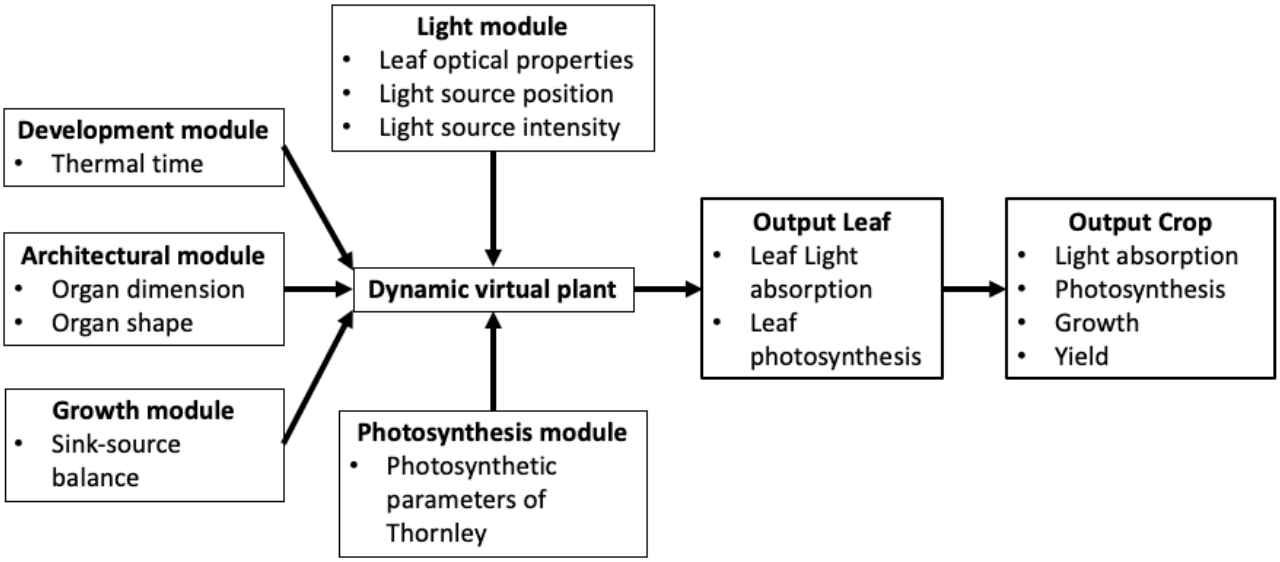

Figure 10. Schematic overview of the FSP model of the dynamic virtual plant including the architectural, light and photosynthesis module.

Any additional details regarding the GroIMP settings can be requested from Dr. Katarina Streit and Dr. Nastassia Vilfan.

3.6.2 Simulations scenarios

After the model was calibrated, three model scenarios were formulated and run for the 62-days.

- **Simple model**: the virtual tomato crop leaf optical properties (transmittance, and reflectance) and photosynthesis parameters including α, ξ and A_{max} are represented by the higher leaf layer parameters (see Appendix A) (Figure 11).
- **Complex OP (Optical Properties) model**: the virtual tomato crop higher leaf layer (rank > 10) and lower leaf layer (rank ≤ 10) are represented by the measured higher and lower layer optical property values, respectively (see Appendix A). The leaf photosynthesis parameters of α, ξ and P_{max} are represented by the higher leaf layer (Figure 11).
- **Complex PS (Photosynthesis) model**: the virtual tomato crop higher leaf layer (rank > 10) and lower leaf layer (rank ≤ 10) are represented by the measured higher and lower layer photosynthesis parameters of α, ξ and A_{max}, respectively (see Appendix A). The leaf optical property parameters are represented by the higher leaf layer (Figure 11).

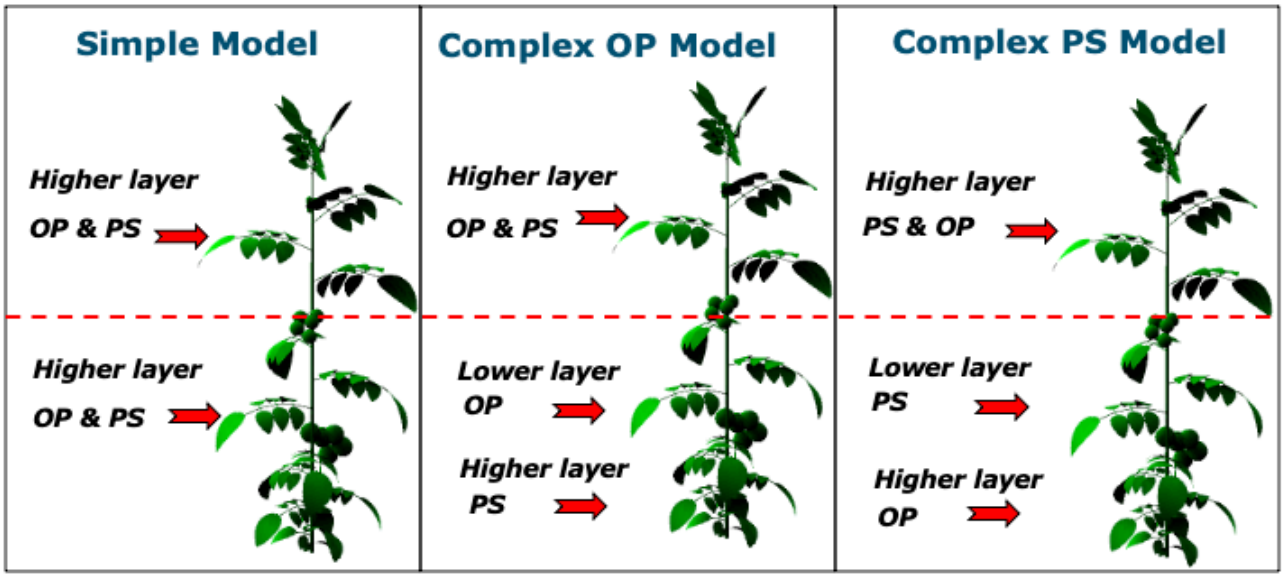

Figure 11. Schematic representation of the virtual tomato crop including higher leaf layer values for optical properties and the photosynthesis parameters for all leaves (Simple model), a virtual tomato crop including a separate higher and lower leaf layer for optical properties (Complex OP model) and a virtual tomato crop including a separate higher and lower leaf layer of photosynthesis parameter (Complex PS model).

The start of each simulation was set to 1/10/2021 and ended on 30/11/2021 (62 days in total). Each model scenario was compared for the total crop light absorption (mol plant $^{-1}$), photosynthesis (mmol CO_2 plant $^{-1}$), growth (g plant $^{-1}$), and yield (g plant $^{-1}$). Moreover, the light phytomer (mol phytomer $^{-1}$ day $^{-1}$) and photosynthesis (mmol CO_2 phytomer $^{-1}$ day $^{-1}$) were compared for each model scenario simulation.

3.7 Data management

Rutger Vreezen was responsible for the data collection and data quality of the leaf optical properties and photosynthesis measurements. Dr. Katarina Streit, Rutger Vreezen, Jasmijn de Jong, and Fotis Palaiochorinos were responsible for the data collection and data quality of the destructive harvest. Moreover, Rutger Vreezen was responsible together with Dr. Nastassia Vilfan and Dr. Katarina Streit for the data storage and backup, archiving and support for the leaf optical properties and photosynthesis data. All data generated was numerical and was saved in an open file (.csv) or excel format (.xlsx). The data storage required was below the 10 GB. The data backup was facilitated by OneDrive for Business (cloud storage) and Microsoft Teams (collaborative platform). There were no intellectual property rights or ethical issues associated with the data. The Microsoft Teams data organisation structure has been provided in the supplementary material (Appendix A).

4. Results

In the following results section the greenhouse climate measurements have been plotted. In addition, the leaf optical properties and net photosynthesis rates have been plotted for each variety and for the higher and lower leaf layer. The fitted Thornley parameters are provided per variety for the higher and lower leaf layer. Moreover, the dry weight, LAI accumulation over time and during the 6th harvest are shown. Finally, the GroIMP scenario results of the total crop light absorption, photosynthesis, growth, yield and phytomer light absorption and phytomer photosynthesis have been shown for each modelling scenario.

4.1 Climate measurements

The daily average air temperature showed constant values during the whole experiment and varied predominantly around the setpoints (Figure 12A & Table 1). The daily average relative humidity initially also stayed predominantly at the setpoint of 70%, however after 15 / 10 / 2021 (18 DAS) the variable approached values closer to the 80% (Figure 12B & Table 1). The daily average CO_2 concentration within the greenhouse initially stayed constant around 400 ppm and progressively increased to 700 ppm starting from the 1/11/2021 (35 DAS) (Figure 12C & Table 1). The solar radiation measurement by the weather station showed high fluctuations during the whole experiment (Figure 13A & Table 1). The PPFD increased from 100 to 188 μmol m^{-2} s^{-1} until 9 / 10 / 2021 (12 DAS) and afterwards stayed constant around 148 μmol m^{-2} s^{-1} (Figure 13B & Table 1). The DLI increased from 5.0 to 9.9 mol m^{-2} day^{-1} until 9 / 10 / 2021 (12 DAS) and afterwards decreased to 6.9 mol m^{-2} day^{-1} at the end of the experiment (Figure 13B & Table 1).

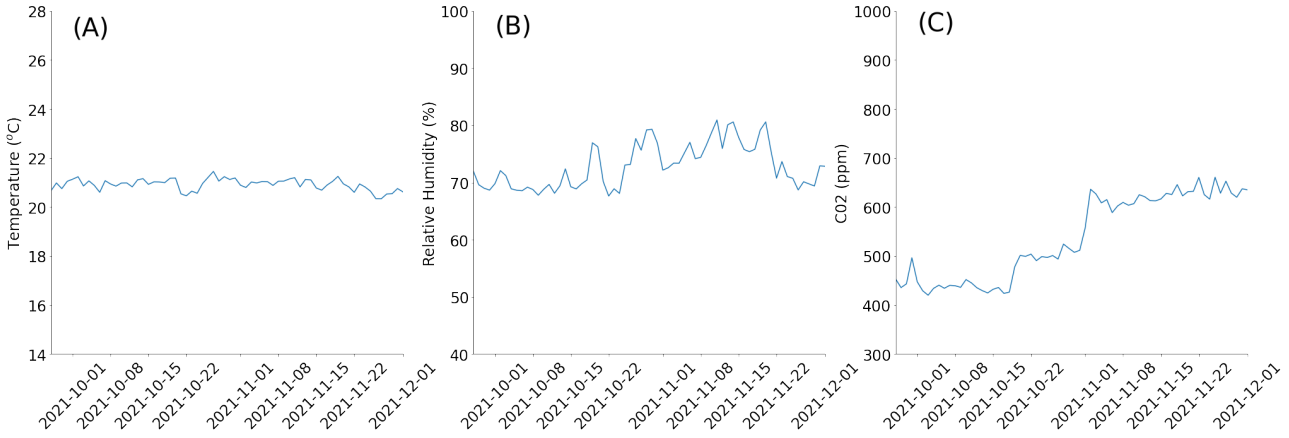

Figure 12: The climate measurements by the Hoogendoorn aspirator box of the daily averages of the air temperature (A), relative humidity (B) and CO_2 - concentration (C) during the experimental trial (64 days).

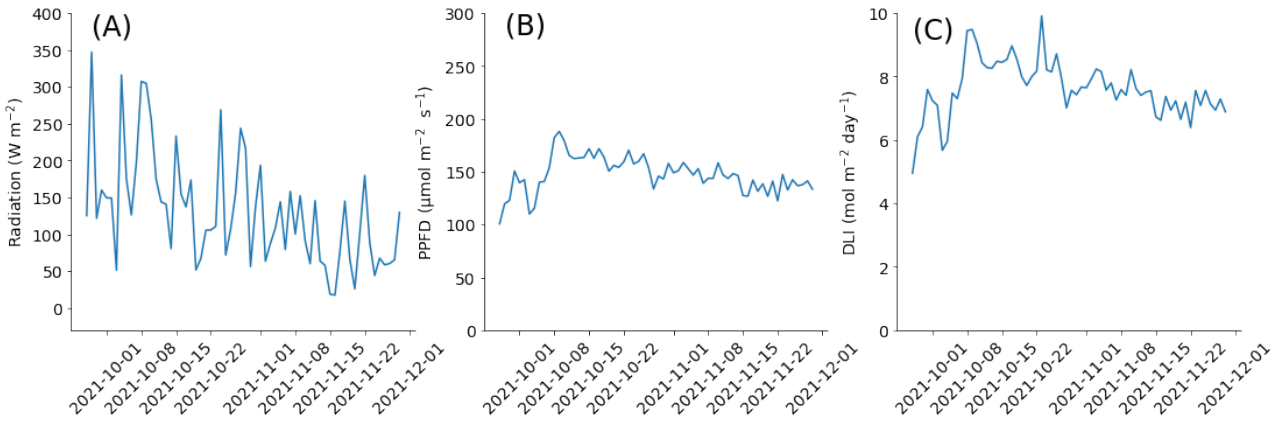

Figure 13: The climate measurements of the Weather station and Sigrow Air+ (ID:62701, see Appendix) of the daily averages of the above greenhouse radiation (A), above canopy PPFD (B) and DLI (C) during the experimental trial (64 days).

Table 1. The climate daily means, maxima, minima and setpoints of the air temperature, relative humidity, and CO_2-concentration of the Hoogendoorn aspirator box, solar top greenhouse radiation of Weather station, canopy PPFD of Sigrow sensors (ID:62701, see Appendix A) during the experiment (64 days).

Climate variable	Temperature [ºC]	Relative Humidity [%]	CO_2 [ppm]	Radiation [W m^{-2}]	PAR [μmol m^{-2} s^{-1}]	DLI [mol m^{-2} day^{-1}]
Mean	20.9	72.9	547	135	148	7.6
Maximum	24.7	91.0	814	691	797	9.9
Minimum	17.3	58.0	398	0	0	5.0
Setpoints	18 – 22	70	700	150 – 250	-	-

4.2 Leaf optical properties

All three tomato varieties showed similar trends of higher adaxial side PAR absorption compared to the abaxial side. Furthermore, all three varieties showed a higher abaxial side PAR reflectance compared to the adaxial side. The leaf PAR transmittance did not show any difference between the adaxial and abaxial leaf side (Figure 14).

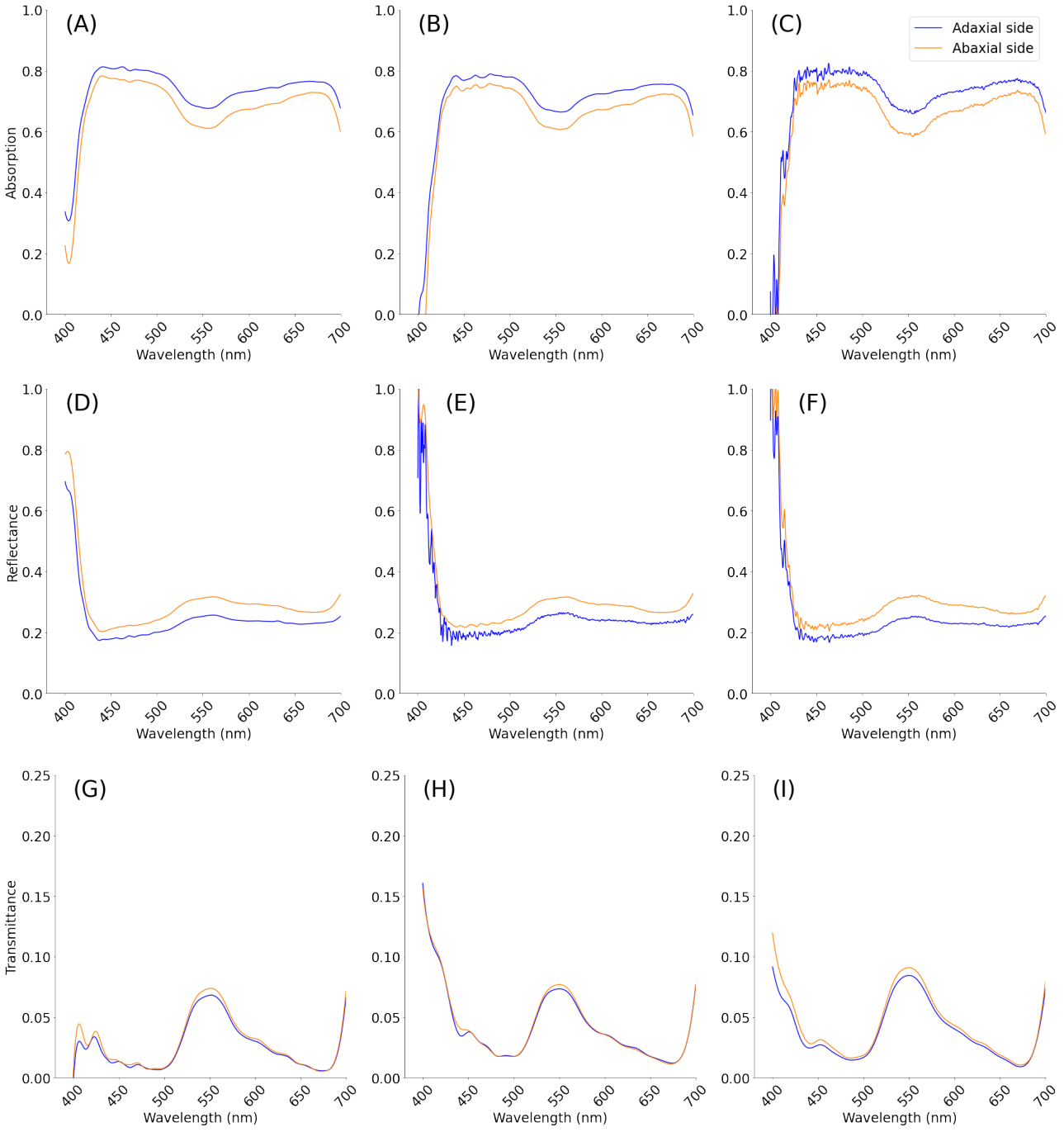

Figure 14. The leaf absorption of the adaxial and abaxial leaf side for three tomato varieties (left: Brioso, middle: Merlice, and right: Moneymaker) plotted against the wavelengths for PAR (400 – 700 nm). The number of replicates can be found in the Appendix A.

Merlice and Moneymaker, showed a similar trend in which the lower layer had a higher or equal average leaf absorption compared to the higher leaf layer. Brioso showed minimal differences in light absorption for the lower leaf layer compared to the higher leaf layer (Figure 15 A, B, C). Moreover, Merlice and Moneymaker showed a higher reflectance for the higher leaf layer compared to the lower leaf layer between 450 – 700 nm. Brioso showed an opposite trend of lower light reflectance of the higher leaf layer compared to the lower leaf layer for 500 – 700 nm (Figure 15 D, E, F). Finally, the Merlice and Moneymaker showed between 450 – 500 nm a higher transmittance for the higher leaf layer compared to the lower leaf layer. Brioso showed a lower light transmittance between 520 – 570 nm for the higher leaf layer compared to the lower leaf layer.

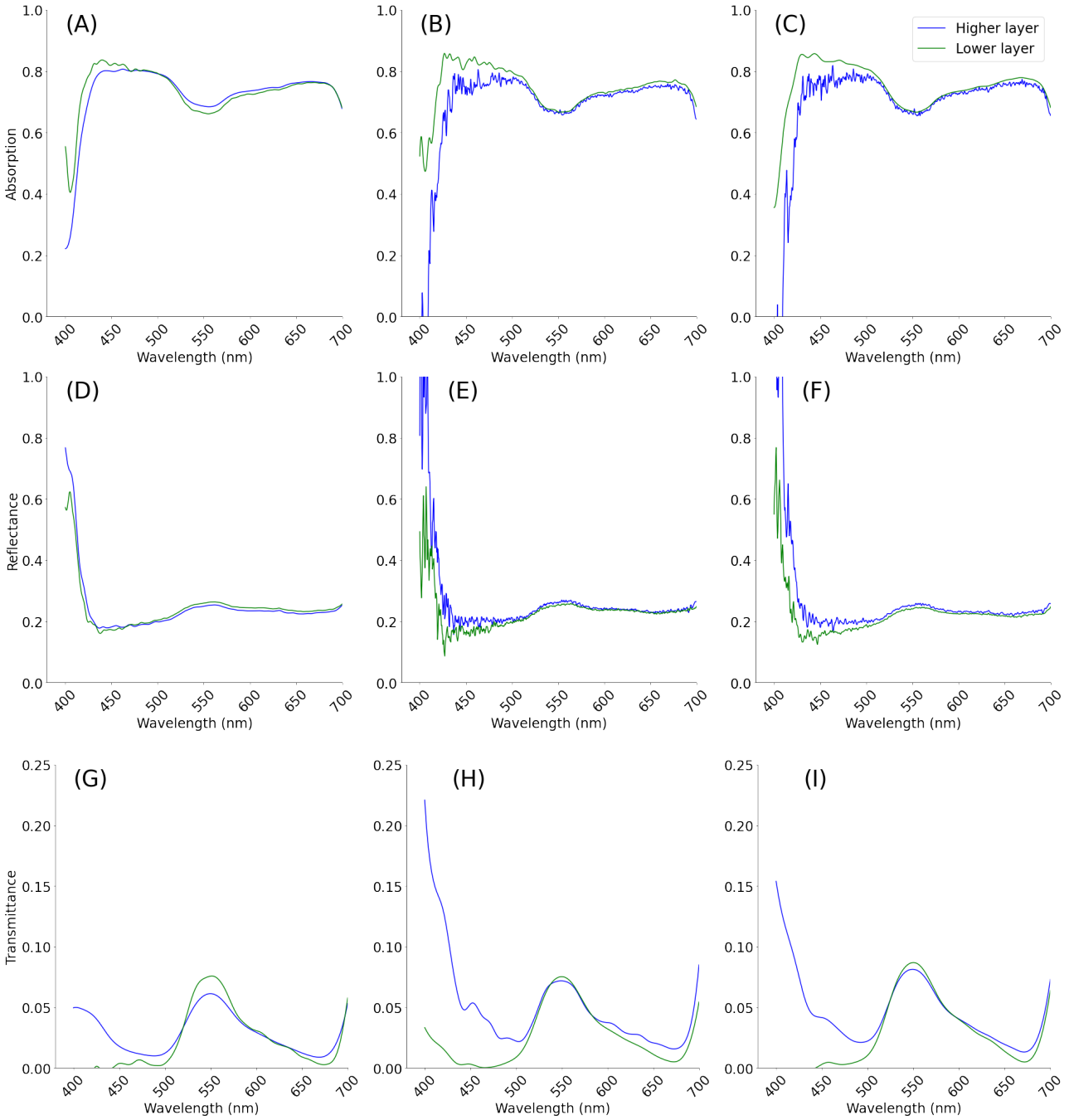

Figure 15. The average adaxial leaf absorption (A, B, C), reflectance (D, E, F) and transmittance (G, H, I) for three tomato varieties (left: Brioso, middle: Merlice, and right: Moneymaker) plotted against the wavelengths for the PAR spectrum (400 – 700 nm) comparing the higher leaf layer (blue) and lower leaf layer (green). The number of replicates can be found in the Appendix A.

For all three varieties there were no significant differences between the average leaf absorption, reflectance or transmittance of the higher leaf layer compared to the lower leaf layer. Merlice and Moneymaker showed a higher average reflectance and transmittance for the higher leaf layer compared to the lower leaf layer. Both varieties showed a lower average absorption for the higher leaf layer compared to the lower leaf layer. Brioso showed the opposite, a higher reflectance and lower absorption of the lower leaf layer. The average transmittance for Brioso did not show any differences (Table 2).

Table 2. The average leaf optical properties (OP) for the spectrum waveband of 450 - 700 nm for three tomato varieties (Brioso, Merlice, Moneymaker) when comparing the higher leaf layer and lower leaf layer using an ANOVA test ($p \leq 0.05$).

Variety	OP	Higher	Lower	P - value
Brioso	Absorption	0.750 ± 0.007	0.743 ± 0.001	0.51
	Reflectance	0.224 ± 0.004	0.231 ± 0.001	0.29
	Transmittance	0.026 ± 0.003	0.026 ± 0.001	0.93
Merlice	Absorption	0.728 ± 0.010	0.749 ± 0.003	0.20
	Reflectance	0.233 ± 0.006	0.224 ± 0.001	0.33
	Transmittance	0.038 ± 0.005	0.027 ± 0.003	0.14
Moneymaker	Absorption	0.735 ± 0.011	0.755 ± 0.005	0.17
	Reflectance	0.226 ± 0.006	0.213 ± 0.003	0.10
	Transmittance	0.039 ± 0.005	0.033 ± 0.004	0.36

4.3 LRC and A / Ci curve

The LRC showed that the net photosynthesis rate of Merlice was significantly lower than both Brioso and Moneymaker for PPFD ranging from 50 – 2000 μmol m^{-2} s^{-1}. Brioso and Moneymaker showed no significant differences in the net photosynthesis rates for similar PPFD (Figure 16A). Moreover, the A / Ci measurements of Merlice showed a significantly lower net photosynthesis rate compared to Brioso for Ci concentrations ranging from 50 – 1400 ppm. Brioso and Moneymaker showed no significant differences in net photosynthesis rates for similar Ci concentrations. Similarly, Moneymaker and Merlice showed no significant differences in net photosynthesis rates for similar Ci concentrations (Figure 16B).

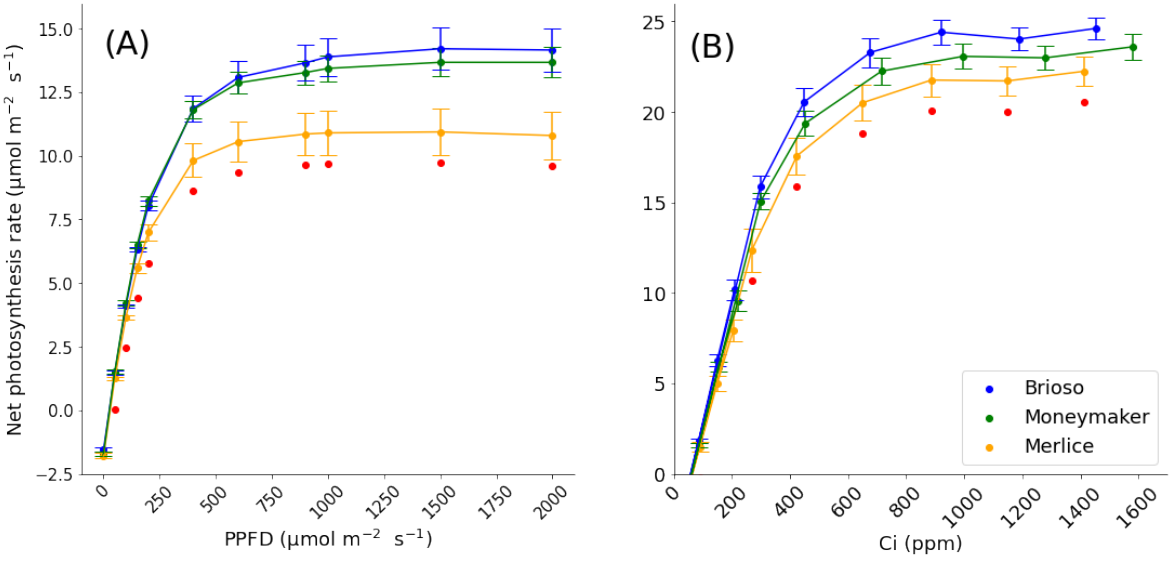

Figure 16. The LRC (A) and A / Ci curve (B) of the net photosynthesis rate for three tomato varieties (Blue: Brioso, orange: Merlice, green: Moneymaker). During the measurements the leaf temperature was kept at 25°C. The error bars indicate the standard error of means. Red points indicate that the varieties' net photosynthesis rate was significantly different ($p \leq 0.05$) compared to the other varieties at the same level of PPFD or Ci . The number of replicates can be found in the Appendix A.

4.3.1 Light Response Curves (LRC) for the higher and lower leaf layer

Brioso and Merlice showed an on average higher net photosynthesis rate for the higher leaf layer compared to the lower leaf layer for PPFD values of 200 – 2000 μmol m^{-2} s^{-1} (Figure 17A & 17B). For Moneymaker the same trend was found for 400 – 2000 μmol m^{-2} s^{-1} (Figure 17C). Contrastingly, Brioso and Merlice showed an on average higher net photosynthesis rate for the lower leaf layer compared to the higher leaf layer for PPFD values of 0 – 150 μmol m^{-2} s^{-1} (Figure 17A & 17B). For Moneymaker the same trend was found for 0 – 400 μmol m^{-2} s^{-1} (Figure 17C). For all three varieties significant differences were found for the net photosynthesis between the higher leaf layer and lower leaf layer at PPFD values of 0 and 50 μmol m^{-2} s^{-1} (see Appendix A).

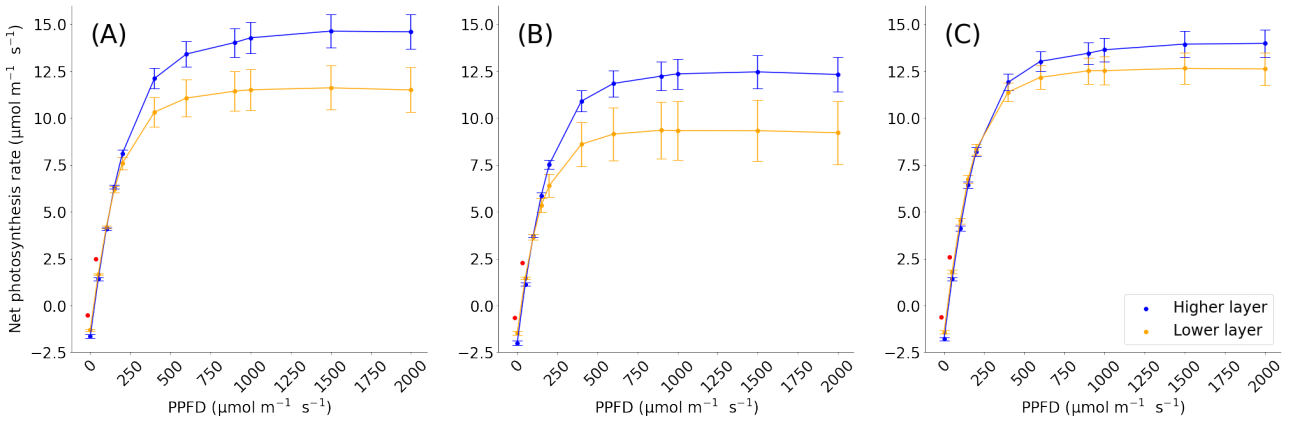

Figure 17. The LRC of the net photosynthesis rate for a range of 0 – 2000 µmol m^{-2} s^{-1} for three tomato varieties (A: Brioso, B: Merlice, C: Moneymaker) divided in a higher leaf layer and lower leaf layer. During the measurements the Ca was kept at 400 PPM and leaf temperature at 25°C. The error bars indicate the standard error of means. Red points indicate significant differences between the higher and lower leaf layer at identical PPFD level ($p \leq 0.05$). The number of replicates can be found in the Appendix A.

It was shown that both α and ξ showed minimal differences between the higher and lower leaf layer for all three tomato varieties. Brioso showed a 25.0% higher A_{sat} of the higher leaf layer compared to the lower leaf layer. Merlice showed a 32.0% higher A_{sat} of the higher leaf layer compared to the lower leaf layer. Moneymaker showed a 9.7% higher A_{sat} of the higher leaf layer compared to the lower leaf layer (Table 3).

Table 3. Non-rectangular hyperbola from the Thornley parameter fitting of α (apparent quantum yield), ξ (curve convexity) and A_{sat} (light-saturated photosynthesis rate) of the higher leaf layer and lower leaf layer derived from fitting the average LRC of each tomato variety (Brioso, Merlice, Moneymaker) to Dr. Nastassia Vilfan linear optimisation model.

Genotype	Layer	α	ξ	A_{sat}
Brioso	Higher	0.053	0.865	15.96
	Lower	0.054	0.877	12.77
Merlice	Higher	0.048	0.917	13.57
	Lower	0.046	0.921	10.28
Moneymaker	Higher	0.053	0.884	15.18
	Lower	0.057	0.896	13.84

4.3.2 A / Ci curve for the higher and lower leaf layer

It was found that Brioso and Merlice had on average a higher net photosynthesis rate for the higher leaf layer compared to the lower leaf layer at Ci levels of 149 – 1453 ppm and Ci levels of 204 – 1411 ppm, respectively (Figure 18 A & B). Moneymaker showed the opposite; an average lower net photosynthesis rate for the higher leaf layer compared to the lower leaf layer at Ci levels of 452 – 1579 ppm (Figure 18 C). Brioso showed significantly higher net photosynthesis between the higher leaf layer and lower leaf layer for 150 and 209 ppm Ci (Figure 18 A).

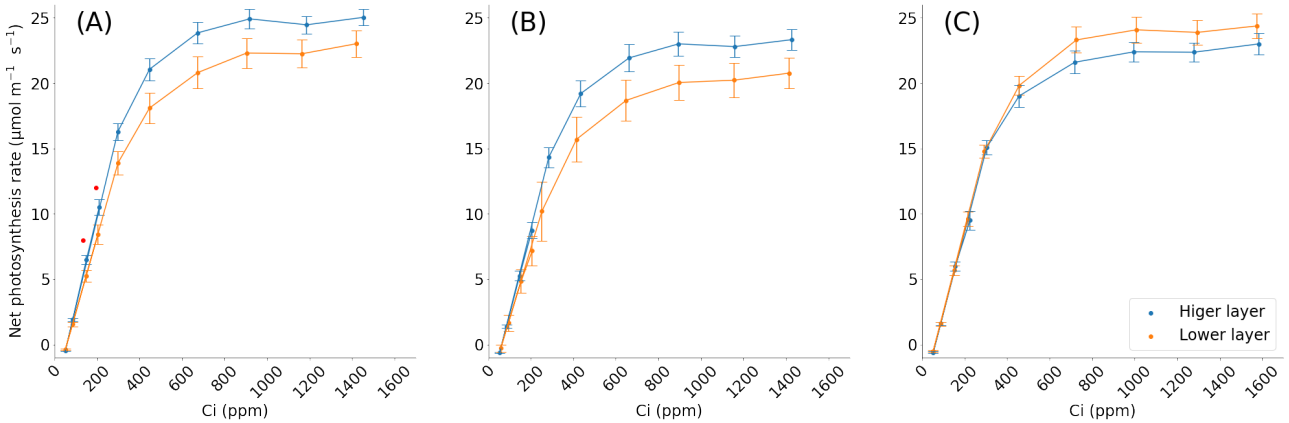

Figure 18. The A / Ci curve of the net photosynthesis rate for the Ci range of 0 to 1600 ppm CO_2 for three tomato varieties (A: Brioso, B: Merlice, C: Moneymaker) divided in a higher leaf layer and lower leaf layer. During the measurements the PPFD light was kept at 1500 µmol m^{-2} s^{-1} and leaf temperature at 25°C. The error bars indicate the standard error of means. Red points indicate significant differences between the higher and lower leaf layer at the same Ci level ($p \leq 0.05$). The number of replicates can be found in the Appendix A.

4.4 Destructive harvest measurements

4.4.1 Dry weight accumulation over 8 weeks

Moneymaker had a significantly lower leaves and stem dry weight between harvest week 4 – 8. Brioso and Merlice showed no significant differences for the leaves and stem dry weight between harvest week 1 – 8 (Figure 19 A & B). Brioso showed a significantly higher dry trusses weight between harvest week 5 to week 8. Merlice and Moneymaker showed no significant differences for the dry trusses weight between harvest week 1 – 8 (Figure 19 C).

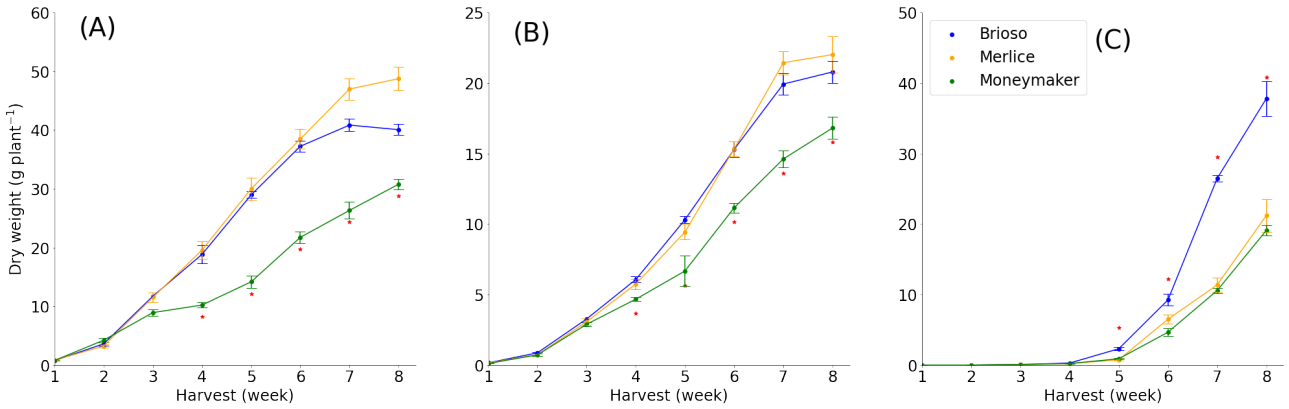

Figure 19. The dry weight accumulation during a 8 weeks growing period of the leaves (A), stem (B) and trusses (C) for three tomato varieties (Brioso, Merlice, and Moneymaker). Red points indicate that the organ dry weight of the variety

was significantly different from organ dry weight of the other two varieties within the same week ($p \leq 0.05$). The number of replicates can be found in the Appendix A.

4.4.2 Dry weight of the 6th destructive harvest

The stem dry weight of Brioso and Merlice were significantly higher compared to Moneymaker. Brioso and Merlices stem dry weight were not significantly different. Moreover, a significantly higher leaves dry weight was found for Brioso and Merlice compared to Moneymaker. Brioso and Merlice leaves dry weight were not significantly different. Finally, Brioso showed a significantly higher trusses dry weight compared to Merlice and Moneymaker. The trusses dry weight of Merlice and Moneymaker were not significantly different (Figure 20 A). It was found that Brioso and Merlice had a significant lower stem partitioning compared to Moneymaker. Moreover, Merlice had a significant higher leaves partitioning compared to Moneymaker. Brioso showed no significant difference in leaves partitioning compared to Merlice and Moneymaker. Finally, no significant differences were found for the trusses partitioning between Brioso, Merlice and Moneymaker (Figure 20 B).

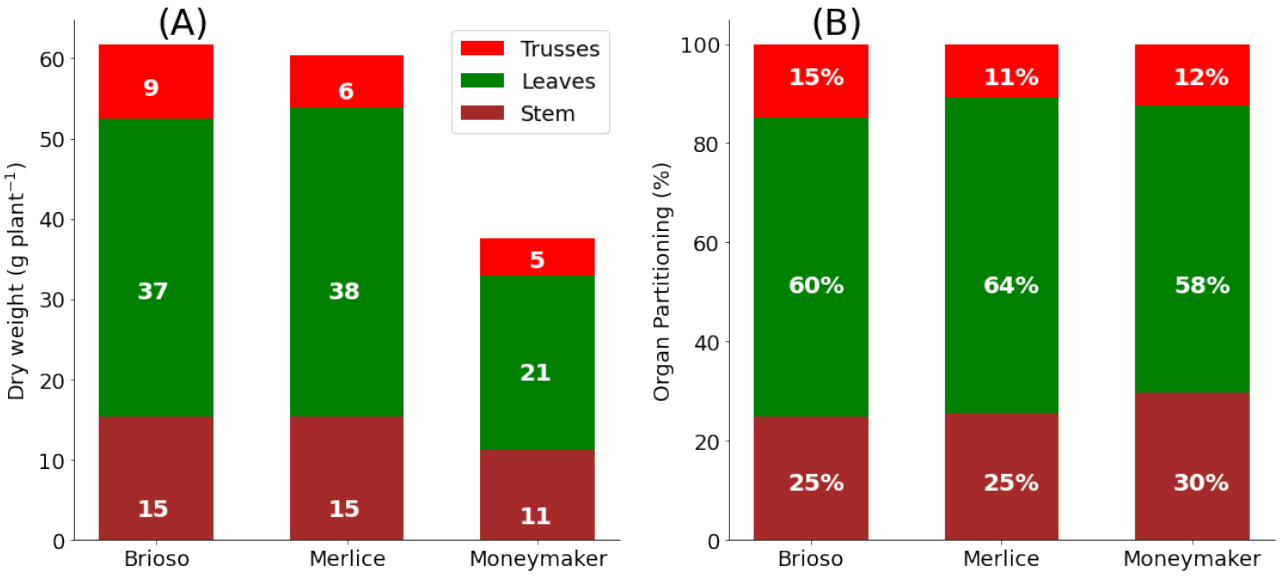

Figure 20. The average plant dry weight (A) and organ partitioning (B) of the stem (brown), leaves (green) and trusses (red) at the 6th harvest week for three tomato varieties (Brioso, Merlice, Moneymaker).

4.4.3 Leaf Area Index over 8 weeks

All three tomato varieties showed a linear trend in the accumulation of the leaf area index (LAI) over the 8 weeks of the experiment. All three tomato varieties showed equal LAI between week 1 – 3. Brioso showed between week 4 and 7 the highest LAI, Moneymaker the lowest LAI and (Figure 21). No significant analysis was conducted for the LAI measurements.

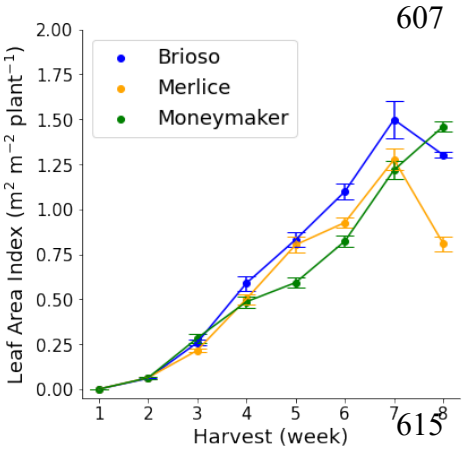

Figure 21. The LAI accumulation during a 8 weeks growing period for three tomato varieties (blue; Brioso, orange; Merlice, and green; Moneymaker). The number of replicates can be found in the Appendix A.

4.5 GroIMP results Merlice

4.5.1 GroIMP results of the total crop light absorption, photosynthesis, growth and yield

The 'Complex OP model' simulation showed a 9.0% higher total accumulated absorbed light, 9.0 % higher gross photosynthesis, 8.9% higher biomass and 8.4% higher yield compared to the 'Simple model'. The 'Complex PS model' simulation showed a 27.6% lower total accumulated absorbed light, 30.1% lower gross photosynthesis, 29.9% lower biomass and 28.8% lower yield compared to the 'Simple model (Figure 22).

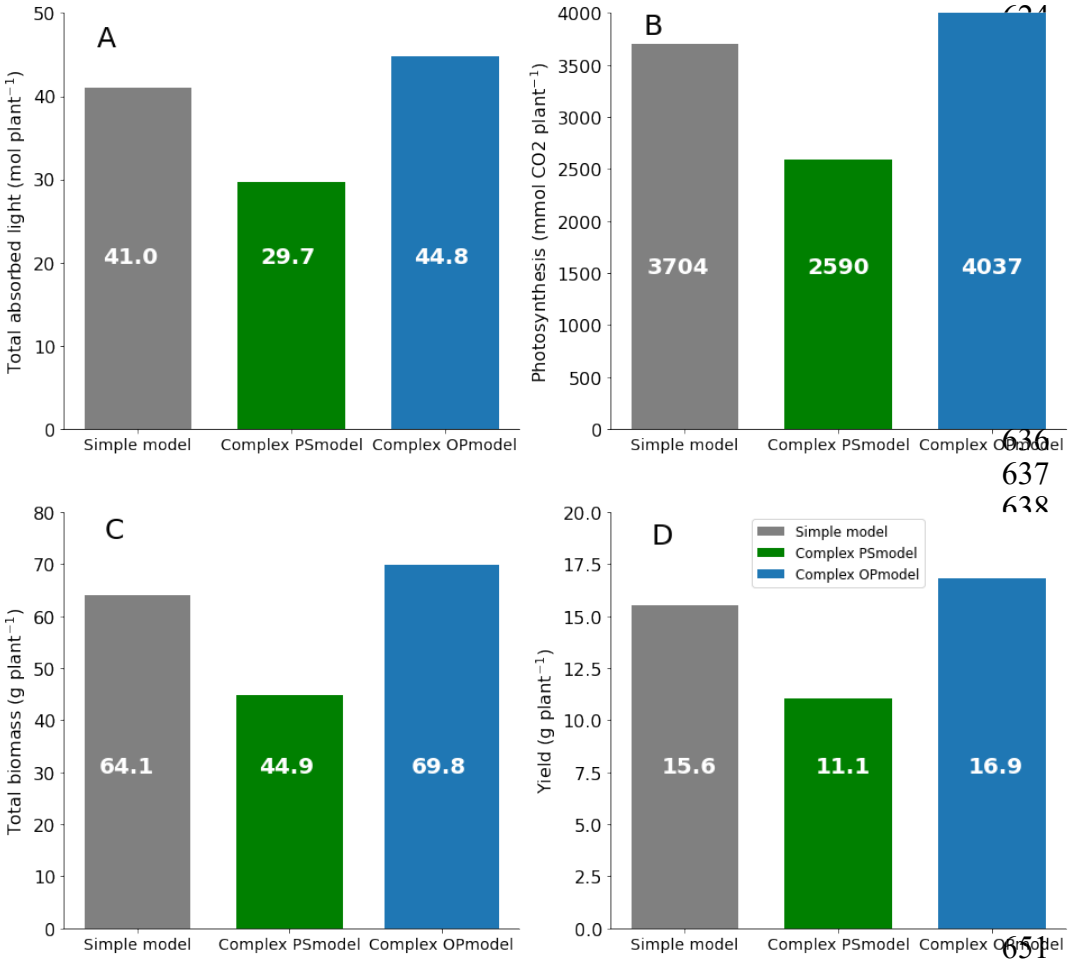

Figure 22. The GroIMP scenario simulations of the total accumulated absorbed light (A), photosynthesis (B), biomass (C) and yield (D) for a the Merlice crop (one plant) over a growing period of 62 days (1032 °C d) using the Twilight flux light model.

4.5.2 GroIMP results of the phytomer light absorption and photosynthesis

All three model scenarios showed a parabolic trend for phytomer light absorption and photosynthesis. The 'Complex OP model' showed the highest light absorption and gross photosynthesis for all phytomer compared to the 'Simple model' and 'Complex PS model'. The 'Complex PS model' showed for all phytomer ranks a lower light absorption and gross photosynthesis compared to the 'Simple model' and 'Complex OP model' (Figure 23).

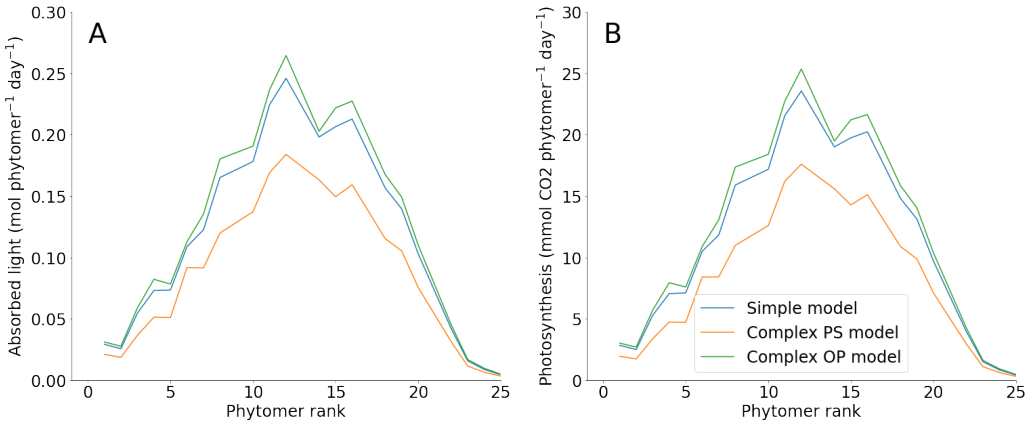

Figure 23. The GroIMP scenario simulation of the absorbed light (A) and assimilates (B) per phytomer rank for Merlice during the last simulation day (day 62; 1032 °C d) using the Twilight flux light model.

5. Discussion

The research aim of this study was to assess the effect of the canopy vertical heterogeneity in leaf optical and and photosynthetic parameters on the simulated virtual tomato crop. The research questions were formulated as: what is the effect of including unique parameters for leaf optical properties (transmittance and reflectance) or leaf photosynthesis (α, ξ and A_{sat}) for the higher and lower leaf layer on the total crop light absorption, photosynthesis, growth, and yield? It was hypothesized that a gradient of leaf optical properties would increase the total crop light absorption due to the on average higher light absorption and lower light transmission of the lower leaf layer (Cui *et al.*, 1991; Kaiser *et al.*, 2019; Poorter *et al.*, 1995). Due to the higher crop light interception also crop photosynthesis, crop growth and yield prediction would be higher. Moreover, it was hypothesized that a gradient of leaf photosynthesis (α, ξ and A_{sat}) would decrease crop photosynthesis rate since the photosynthetic capacity (A_{sat}) of the lower leaf layer is lower compared to the higher leaf layer. Thereby also decreasing growth and yield prediction. Three model scenarios were formulated: the 'Simple model' (all crop leaves had the leaf optical properties and photosynthetic parameters of the higher leaf layer), the 'Complex OP model' (the higher and lower leaf layer had unique parameters for optical properties and all leaves had the photosynthetic parameters of the higher leaf layer), and 'Complex PS model' (the higher and lower leaf layer had unique photosynthetic parameters and all leaves had the optical properties parameters of the higher leaf layer). At the date of writing this research the GroIMP calibration was not fully finalized. For that reason, the model simulation results could not yet be compared to the measured destructive harvest (Figure 19 & 20).

5.1 The effect of including a vertical gradient of leaf optical properties

For all three varieties a higher absorption, lower reflectance and equal transmittance was found for the adaxial leaf side compared to the abaxial leaf side (Figure 14). Mooney & Lieth (1985) also showed these differences in leaf absorption, reflectance and transmittance for the adaxial and abaxial leaf side. It was found that Merlice and Moneymaker showed 28.9% and 15.4% lower leaf transmittance for the leaf adaxial side of the lower leaf layer compared to the higher leaf layer. Moreover, Merlice and Moneymaker showed for the leaf adaxial side

692 a 2.9 % and 2.7 % lower average leaf absorption and 3.9 % and 5.8 % higher average reflectance for the higher
693 leaf layer compared to the lower leaf layer, respectively (Table 2 & Figure 15). The same trend in differences
694 were found for the abaxial leaf side (see Appendix A). These findings are in line with the findings of Poorter
695 *et al*. (1995) that showed for some tropical trees species a similar trend of top canopy leaves having a lower
696 light absorption and higher transmittance compared to the understory and mid-canopy leaves. Poorter *et al*.
697 (1995) showed no differences in light reflectance of the canopy, compared to the mid-canopy and understory.
698 Also in this study the relfectane differences between higher and lower leaf layer were found to be small and
699 non-significant. Interestingly, Brioso showed the opposite trend; a slight (0.9%) lower leaf absorption and
700 higher reflectance (3.1%) of the lower leaf layer compared to the higher leaf layer. The different leaf absorption
701 was considered to be minimal and the higher light reflectance was suggested to be a variety specific trait. When
702 comparing the 'Simple model' scenario to 'Complex OP model' scenario simulation it was found that the
703 'Complex OP model' had a 9.0 % higher total accumulated absorbed light, 9.0 % higher gross photosynthesis,
704 8.9 % higher biomass and 8.4 % higher yield compared to the 'Simple model' (Figure 22). This was in line
705 with the hypothesis that suggested that by including the lower leaf layer optical properties in the crop model
706 the overall crop light absorption and therefore photosynthesis, growth, and yield would increase. Therefore, it
707 has been shown that the simulation of unique optical properties for the higher and lower leaf layer in the digital
708 tomato crop has a large effect on the functionality of the digital tomato crop.
709
710 ## 5.2 The effect of including a vertical gradient of leaf photosynthetic parameters
711 All three varieties showed a higher net photosynthesis rate for the higher leaf layer compared to the lower leaf
712 layer for the LRC between a PPFD of 200 – 2000 μmol m^{-2} s^{-1} (Figure 17). In addition, Brioso and Merlice
713 showed a higher net photosynthesis rate for the higher leaf layer compared to the lower leaf layer in A/Ci curve
714 between Ci of 200 – 1500 ppm. Interestingly, in the A/Ci curve Moneymaker showed a trend of higher net
715 photosynthesis rates for the lower leaf layers. However, the differences in net photosynthesis between both
716 layers were considered minimal, therefore no further conclusions were drawn from these measurements
717 (Figure 18). Furthermore, all three varieties showed significantly lower net photosynthesis rates of the higher
718 leaf layer compared to the lower leaf layer in the LRC between a PPFD of 0 – 50 μmol m^{-2} s^{-1} (Figure 17 &
719 see Appendix A). This can be explained by the fact that the higher leaf layer had a higher dark respiration rate
720 compared to the lower leaf layer (see Appendix A). These finding are also in line with Acock *et al*. (1978) that
721 showed that the uppermost leaf layer and middle layer had aproximately a 7 and 4 times higher dark respiration
722 rate compared to the lowest leaf layer, respectivily. In the GroIMP simulations the leaf dark respiration was
723 not considered, but the crop respiration was calculated as a fixed fraction of the available assimilates. Therefore
724 this effect of higher dark respiration rate of the higher leaf layer was not included in the model results.
725 However, at higher levels of PPFD (> 200 μmol m^{-2} s^{-1}) the differences in net photosynthesis between the
726 higher and lower layer were substantial larger. Therefore, it is expected that the lower net photosynthesis rates
727 of the higher leaf layer compared to the lower leaf layer at PPFD levels below 200 μmol m^{-2} s^{-1} had a minimal
728 effect on the overall crop net photosynthesis. Moreover, Brioso, Merlice, and Moneymaker showed that the

729 higher leaf layer had a 25%, 32.0%, and 9,7% higher fitted A_{sat} compared to the lower leaf layer, respectively
730 (Table 3). These results are in line with the research of Trouwborst *et al*. (2011) and Acock *et al*. (1978), who
731 also showed that within the crop the photosynthetic capacity progressively decreases downwards due to low
732 light acclimation of the shaded lower leaves. For the fitted photosynthetic parameter α and ξ no large
733 differences were found for the higher and lower leaf layer for all three varieties. Acock *et al*. (1978) also did
734 not show vertical differences in α at different heights within the tomato crop. As result of the 32.0% lower
735 A_{sat} of the lower leaf layer the estimations for crop gross photosynthesis (30.1 %), crop light absorption (27.6
736 %), total biomass (29.9 %) and yield (28.8 %) of the 'Complex PS' model were substantially lower compared
737 to the 'Simple model' (Figure 22). Therefore, it has been shown that the simulation of unique photosynthetic
738 paramters for the higher and lower leaf layer in the digital tomato crop has a large effect on the functionality
739 of the digital tomato crop.
740

741 ## 5.3 Vertical differences in leaf stomata conductance

742 Interestingly, all three tomato varities showed a higher stomata conductance of the higher leaf layer compared
743 to the lower leaf layer for the LRC and A/Ci curve (see Appendix A). This effect could (partially) explain the
744 higher net photosynthesis rates of the higher leaf layer. Namely, Du *et al*. (2018) showed that for tomato
745 limitations in stomata conductances were responsible for 60% of the reduced net photosynthesis. Du *et al*.
746 (2018) also showed that a reduced mesophyl conductance had a negative effect on the net photosynthesis rate
747 and the extent of the effect was mostly cultivar specific. Due to the lower stomata conductance and potentially
748 the mesophyl conductance the CO_2 transport into the leaf was limited and thereby leaf photosynthesis rate was
749 limited as well for the lower leaf layers.
750

751 ## 5.4 Delayed CO_2 supplementation

752 During the experiment duration the greenhouse climate variables were highly controlled. The air temperature
753 and relative humidity were sufficiently close to the greenhouse climate settings. These variables did not reach
754 any critical maximum or minimum values that could have compromised the growth of the tomato crop (Figure
755 12 & Table 1). However, the CO_2 supplementation was only active after the 1/11/2021 (35 DAS) and
756 progressively increased from 400 ppm to 700 ppm (Figure 12 C). This left the first 35 days without CO_2
757 supplementation. The first photosynthesis measurements were conducted between the 3/11/2021 (37 DAS)
758 until the 25/11/2021 (59 DAS). During the Li6800 measurements the intercellular CO_2 was determined by the
759 LRC and A/Ci program. Therefore, an immediate effect of the increased ambient CO_2 concentration inside the
760 greenhouse on leaf photosynthesis was not expected. However, it has been shown that the photosynthetic
761 capacity declined in tomato after 5 – 7 weeks of growth in high CO_2 concentration as a result of rubisco
762 deactivation (Besford *et al*., 1990). Nonetheless, in the sixth (36 – 42 DAS) and seventh week (43 – 49 DAS)
763 of the experiment no decrease in photosynthetic capacity was found. For that reason, it was assumed that the
764 increase in ambient CO_2 concentration inside the greenhouse had no substantial effect on the net photosynthesis
765 measurements. Thornley parameters were fitted to the LRC. During the light response curve, the CO_2

concentration was to 400 ppm. Therefore, it can be expected that the actual leaf photosynthesis rate of tomato leaves was higher due to the higher CO_2 concentrations ranging from 400 – 700 nm after 1/11/2021 (35 DAS). This effect of increased photosynthesis and therefore growth after the 1/11/2021 (35 DAS) had not been included in the model estimations.

5.5 The small virtual crop

During this experiment the tomato plants stayed relatively small (maximum height of 1.5 m) and on average each tomato plant had during the whole experiment LAI below 2.0 (Figure 21). Therefore, it can be concluded that for a large part of the experiment the crop still had an open canopy. At a higher LAI (> 3.0) the crop canopy is closed, and the higher canopy leaves will (partially) shade the leaves of the lower layers. As a result, the light levels exponentially decrease from the top to the bottom of the crop (Sinclair, 1967; Slattery & Ort, 2021). Therefore, as Sarlikioti (2011) also showed, in that situation the upper canopy leaves intercept the majority of the available light compared to the lower canopy leaves. As result of the exponential decay of light Acock *et al*. (1978) showed that the uppermost layer of a large tomato crops, consisted of 23% of the leaf total area, contributed 66% of the total amount of assimilates. This shows that in a tomato crop with a high LAI (> 3.0) the higher leaf layer plays the dominant role in the determination of total crop light absorption and gross photosynthesis. In small crops that consist of a low LAI (< 2.0), it is expected that the lower leaf layer still plays an important role in the total crop light absorption and yield because of the lack of (partial) shading effect of the higher leaf layer. This is supported by the GroIMP model simulation that showed that all three model scenarios had the highest light absorption and gross photosynthesis in the middle of the crop (rank 1 – 15). Therefore, the leaf rank light absorption and gross photosynthesis showed a parabolic rather than an exponential trend (Figure 23). Since in Dutch commercial greenhouses tomatoes are typically grown with a high LAI (3.0 – 4.0) during most of the growing season as mentioned in Heuvelink *et al*. (2005), it is suggested that the effect of including leaf optical properties and photosynthetic parameters could have a smaller effect on the functionality of larger tomato crops.

5.6 Dynamic instead of static leaf layer simulation

In this research during the model simulations the higher leaf layer (rank > 10) and lower leaf layer (rank ≤ 10) were determined by the predetermined phytomer rank. This implied that during the initial simulated growth of the virtual tomato crop until rank 10 all leaves had the lower leaf optical properties or photosynthetic parameters for the 'Complex OP' model and 'Complex PS model', respectively. After the virtual growth succeeded rank 10 all higher leaf layer optical properties and photosynthetic parameters were applied for each model scenario. However, in a real crop is expected that the ranks belonging to the higher and lower leaf layer change over time as result of the continuing vertical growth. It is therefore expected that the higher and lower leaf layer determination should be conducted on a dynamic basis. It is suggested to include this dynamic behavior of the leaf layers by counting the leaf phytomer rank number from the top to bottom. Thereby, the

802 determination of the higher and lower leaf layer is not affected by the increase in vertical plant growth over
803 time.
804
805 ## 6. Conclusions
806 In this study it was shown that the leaf optical and photosynthetic parameters were substantially dissimilar at
807 two different leaf layers and had a large effect on the FSP model estimations for crop light absorption, gross
808 photosynthesis, growth, and yield predictions. The lower leaf layer showed a 2.9 % higher light absorption,
809 3.9 % lower reflectance, 28.9% lower light transmittance and a 32% lower light saturated photosynthesis rate
810 compared to higher leaf layer for the Merlice variety. Including unique optical properties for the higher and
811 lower leaf layer ('Complex OP model') resulted in a higher model estimation of crop light absorption (9.0 %),
812 crop gross photosynthesis (9.0 %), growth (8.9 %), and yield (8.4 %). On the other hand, including unique
813 photosynthesis parameters for the higher and lower leaf layer ('Complex PS model') resulted in a lower model
814 estimation of crop gross photosynthesis (30.1 %), crop light absorption (27.6 %), total biomass (29.9 %) and
815 yield (28.8 %). The findings of this study concluded that representing the crop vertical diversity in leaf optical
816 and photosynthetic parameters can greatly alter the FSP model predictions for crop light absorption, gross
817 photosynthesis, growth, and yield. For that reason, it is advised to consider this vertical heterogeneity in optical
818 and photosynthetic properties in FSP model simulations. Especially for crops that increase substantially in
819 length over the growing season such as sweet pepper and cucumber. Furthermore, it was concluded that the
820 leaf layer determination would be done optimally on a dynamic basis. It is therefore suggested to include this
821 dynamic behaviour by counting the leaf phytomer from top to bottom instead of from bottom to top for the
822 optical properties and photosynthesis measurements. It is also concluded that in a tomato crop with a high
823 LAI (> 3.0) the higher leaf layer could play a dominant role in the crop light interception and photosynthesis
824 and therefore the effect of including the distant parameters for leaf optical properties and photosynthesis of the
825 lower leaf layer could have a smaller effect. Therefore, further research would be required to evaluate the effect
826 of the simulation of larger tomato crops.
827
828 ## 7. Recommendations
829 It has been shown that the leaf optical properties and leaf photosynthetic parameters are highly dependent on
830 the leaf vertical position within the tomato crop. During the eight experimental weeks the optical properties
831 and photosynthesis measurements were conducted during 2 and 4 consecutive weeks, respectively. Hereby,
832 focussing on three tomato varieties every week. To generate a more accurate description of the relationship of
833 leaf optical properties and photosynthetic parameters and the vertical position within the crop it could be
834 recommended to focus on one variety. As result it would be feasible to measure more different leaf ranks for
835 this variety and generate more extensive vertical gradient of the optical properties and photosynthetic
836 parameters within the crop. In that way the optical and photosynthetic parameters of the phytomer ranks that
837 have not been measured can be estimated by interpolations for in the simulated virtual tomato crop. In addition,
838 when conducting further experiments at the NPEC research facility it would be beneficial to install reliable

PPFD measurements. Namely, during this experiment the PAR bars were not correctly calibrated and the Sigrow sensors turned out to measure PPFD and DLI inaccurately as can be found in the quantum response curve (see Appendix A). For that reason, the PPFD and DLI could only be used as rough estimation of the above canopy light environment. During the experiment there were effectively three days of delayed watering (26/10/2021, 7/11/2021, 24/11/2021). No photosynthesis measurements were conducted during days with delayed watering. Moreover, during all photosynthesis measurements the leaf stomata conductance was above the threshold of 0.10 μmol m^{-2} s^{-1} for both the LRC and A/Ci (see Appendix A). In addition, the net photosynthesis rates of the LRC and A/Ci curve have been compared to the study of Pan *et al*. (2020) and were in the same order of magnitude (Figure 16). Therefore, it was assumed that the net photosynthesis rates were not affected by the delayed watering at any measurement. However, it is expected that due to the three days of delayed watering, the plant height, number of leaves and number of fruits per plant were reduced to an extent (Pervez *et al*., 2009). In the GroIMP simulations this drought stress was not included. Therefore, for future research it could be interesting to evaluate and model the effect of the drought stress during the three days of delayed watering. Because, without including the drought stress it is expected that the model simulation would overestimate the growth and yield.

8. Acknowledgement

I am grateful to my super visors Dr. Nastassia Vilfan and Dr. Katarina Streit for their guidance and support in the Python data-analysis and GroIMP modelling and the compressive feedback on the report. Moreover, I want to thank Dr. Katarina Streit, Jasmijn de Jong, and Fotis Palaiochorinos for their contribution to the experimental harvesting efforts and being great working partners.

9. References

Allen, M. T., Prusinkiewicz, P., & DeJong, T. M. (2005). Using L-systems for modeling source-sink interactions, architecture and physiology of growing trees: The L-PEACH model. *New Phytologist*, *166*(3), 869–880. https://doi.org/10.1111/j.1469-8137.2005.01348.x

Besford, R. T., Ludwig, L. J., & Withers, A. C. (1990). The greenhouse effect: Acclimation of tomato plants growing in high CO2, photosynthesis and ribulose-1, 5-Bisphosphate carboxylase protein. *Journal of Experimental Botany*, *41*(8), 925–931. https://doi.org/10.1093/jxb/41.8.925

Bongers, F. J., Pierik, R., Anten, N. P. R., & Evers, J. B. (2018). Subtle variation in shade avoidance responses may have profound consequences for plant competitiveness. *Annals of Botany*, *121*(5), 863–873. https://doi.org/10.1093/aob/mcx151

Chelle, M, & Andrieu, B. (2007). Modelling the Light Environment of Virtual Crop Canopies. *Functional-Structural Plant Modelling in Crop Production*, 75–89. https://doi.org/10.1007/1-4020-6034-3_7

Chelle, Michaël. (2005). Phylloclimate or the climate perceived by individual plant organs: What is it? How to model it? What for? *New Phytologist*, *166*(3), 781–790. https://doi.org/10.1111/j.1469-8137.2005.01350.x

876 Cieslak, M., Lemieux, C., Hanan, J., & Prusinkiewicz, P. (2008). Quasi-Monte Carlo simulation of the light
877 environment of plants. *Functional Plant Biology*, *35*(10), 837–849. https://doi.org/10.1071/FP08082
878 Cui, M., Vogelmann, T. C., & Smith, W. K. (1991). Chlorophyll and light gradients in sun and shade leaves
879 of Spinacia oleracea. *Plant, Cell & Environment*, *14*(5), 493–500.
880 Department Ecoinformatics. (2011). *GroIMP software*. Biometrics and Forest Growth, Georg-August
881 University of Göttingen. http://wwwuser.gwdg.de/~groimp/grogra.de/software/groimp/index.html
882 Du, Q., Xing, G., Jiao, X., Song, X., & Li, J. (2018). Stomatal responses to long-term high vapor pressure
883 deficits mediated most limitation of photosynthesis in tomatoes. *Acta Physiologiae Plantarum*, *40*(8),
884 1–12. https://doi.org/10.1007/s11738-018-2723-7
885 Evers, J. B., Vos, J., Yin, X., Romero, P., Van Der Putten, P. E. L., & Struik, P. C. (2010). Simulation of
886 wheat growth and development based on organ-level photosynthesis and assimilate allocation. *Journal*
887 *of Experimental Botany*, *61*(8), 2203–2216. https://doi.org/10.1093/jxb/erq025
888 Evers, J., & Marcelis, L. (2019). *Functional—structural plant modeling of plants and crops*. 45–68.
889 https://doi.org/10.19103/as.2019.0061.02
890 Evers, Jochem B., Letort, V., Renton, M., & Kang, M. (2018). Computational botany: Advancing plant
891 science through functional-structural plant modelling. *Annals of Botany*, *121*(5), 767–772.
892 https://doi.org/10.1093/aob/mcy050
893 Godin, C., & Sinoquet, H. (2004). Functional – structural plant modelling. *The New Phytologist 166(3), 705–*
894 *8. doi*, 791–800.
895 Goudriaan, J., & Van Laar, H. H. (2012). *Modelling potential crop growth processes: textbook with*
896 *exercises*. Springer Science & Business Media.
897 Hemmerling, R., Kniemeyer, O., Lanwert, D., Kurth, W., & Buck-Sorlin, G. (2008). The rule-based
898 language XL and the modelling environment GroIMP illustrated with simulated tree competition.
899 *Functional Plant Biology*, *35*(10), 739–750. https://doi.org/10.1071/FP08052
900 Heuvelink, E., Bakker, M. J., Elings, A., Kaarsemaker, R. C., & Marcelis, L. F. M. (2005). Effect of leaf area
901 on tomato yield. Acta Horticulturae. *Acta Horticulturae*, *691*, 43–50.
902 Heuvelink, Ep. (2018). *Tomato. 2nd edition. Crop Production Science in Horticulture* (Ep Heuvelink (Ed.);
903 2nd ed.). Wageningen University & Research.
904 Hopkins, W., & Hüner, N. (2009). *Introduction to Plant Physiology* (4th editio). John Wiley & Sons, Inc.
905 *Index of/GroIMP*. (2011). Biometrics and Forest Growth, Georg-August University of Göttingen.
906 http://ufgb966.forst.uni-goettingen.de/GroIMP/
907 Kaiser, E., Weerheim, K., Schipper, R., & Dieleman, J. A. (2019). Partial replacement of red and blue by
908 green light increases biomass and yield in tomato. *Scientia Horticulturae*, *249*(November 2018), 271–
909 279. https://doi.org/10.1016/j.scienta.2019.02.005
910 Kurth, W., Kniemeyer, O., & Buck-Sorlin, G. (2004). *Unconventional Programming Paradigms*. Springer.
911 Kuusk, A. (2001). A two-layer canopy, reflectance model. *Journal of Quantitative Spectroscopy and*
912 *Radiative Transfer*, *71*(1), 1–9. https://doi.org/10.1016/S0022-4073(01)00007-3

913 Marcelis, L. F. M. (1996). Sink strength as a determinant of dry matter partitioning in the whole plant.
914 *Journal of Experimental Botany 47*, *1281–91*(Special_Issue.1281), doi:10.1093/jxb/47.
915 Marcelis, L. F. M., Heuvelink, E., & Goudriaan, J. (1998). Modelling biomass production and yield of
916 horticultural crops: A review. *Scientia Horticulturae*, *74*(1–2), 83–111. https://doi.org/10.1016/S0304-
917 4238(98)00083-1
918 Mooney, H., & Lieth, H. (1985). *Photosynthesis during leaf development* (Z. SESTAK & D. Prof. RNDr.
919 PhMr. Miroslav Penka (Eds.)). Dr W. Junk Publishers.
920 Muller, J., Wernecke, P., Braune, H., & Diepenbrock, W. (2007). Photosynthesis And Carbon Balance.
921 *Functional-Structural Plant Modelling in Crop Production*, *1976*, 91–101. https://doi.org/10.1007/1-
922 4020-6034-3_8
923 NPEC. (2022). *WUR is working on Digital Twins for tomatoes, food, and farming*. NPEC.
924 https://www.npec.nl/experiments/digital-twin-project-virtual-tomato-crops/
925 Pan, T., Wang, Y., Wang, L., Ding, J., Cao, Y., Qin, G., Yan, L., Xi, L., Zhang, J., & Zou, Z. (2020).
926 Increased CO2 and light intensity regulate growth and leaf gas exchange in tomato. *Physiologia*
927 *Plantarum*, *168*(3), 694–708. https://doi.org/10.1111/ppl.13015
928 Pervez, M., Ayub, C., Khan, H., Shahid, M., & Ashraf, I. (2009). Effect of Drought Stress on Growth, Yield
929 and Seed. *Journal Agribussines Science*, *46(3)*(Quality of tomato park), 174–178.
930 Poorter, L., Oberbauer, S. F., & Clark, D. B. (1995). Leaf Optical Properties Along a Vertical Gradient in a
931 Tropical Rain Forest Canopy in Costa Rica. *American Journal of Botany*, *82*(10), 1257–1263.
932 Reinhardt, D., & Kuhlemeier, C. (2002). Plant architecture. *EMBO Reports*, *3*(9), 846–851.
933 https://doi.org/10.1093/embo-reports/kvf177
934 Sarlikioti, V. (2011). *Modelling and Remote Sensing of Canopy Light Interception and Plant Stress in*
935 *Greenhouses*. Wageningen University, Wageningen, The Netherlands. https://edepot.wur.nl/183133
936 Schlichting, C. D. (1986). the Evolution of Phenotypic Plasticity in Plants. *Annual Review of Ecology and*
937 *Systematics*, *17*(1), 667–693. https://doi.org/10.1146/annurev.es.17.110186.003315
938 Sinclair, T. R. (1967). "A Model for Simulating Photosynthesis in Plant Communities" by W.G. Duncan,
939 R.S. Loomis, W.A. Williams, and R. Hanau, Hilgardia (1967) 38:181–205. *Crop Science*, *59*(1), 15–18.
940 https://doi.org/10.2135/cropsci2018.07.0467
941 Slattery, R. A., & Ort, D. R. (2021). Perspectives on improving light distribution and light use efficiency in
942 crop canopies. *Plant Physiology*, *185*(1), 34–48. https://doi.org/10.1093/PLPHYS/KIAA006
943 *The Python Standard Library*. (2022). Python Software Foundation. https://docs.python.org/3/library/
944 Thornley, J. H. M. (1998). Dynamic Model of Leaf Photosynthesis with Acclimation to Light and Nitrogen.
945 *Oxford University Press*, *81*(3), 421–430.
946 Trouwborst, G., Hogewoning, S. W., Harbinson, J., & van Ieperen, W. (2011). The influence of light
947 intensity and leaf age on the photosynthetic capacity of leaves within a tomato canopy. *Journal of*
948 *Horticultural Science and Biotechnology*, *86*(4), 403–407.
949 https://doi.org/10.1080/14620316.2011.11512781

Vos, J., Evers, J. B., Buck-Sorlin, G. H., Andrieu, B., Chelle, M., & De Visser, P. H. B. (2010). Functional-structural plant modelling: A new versatile tool in crop science. *Journal of Experimental Botany*, *61*(8), 2101–2115. https://doi.org/10.1093/jxb/erp345

Wald, L. (2018). Basics in Solar Radiation At Earth Surface. *Hal*, *January*, 57. https://doi.org/10.13140/RG.2.2.36149.93920

10. Appendix A

10.1 Definitions

Table A1. Definitions

Word	Definition
Development	Consecutive creation of vegetative or reproductive plant organs (Ep Heuvelink, 2018).
Direct sunlight	The shortwave irradiation coming from the solid angle of the sun. The sun waves can be assumed being parallel to each other (Wald, 2018).
Growth	Irreversible enlargement of plant or organ dimension over time quantified in mass, length, width, or area (Ep Heuvelink, 2018).
Indirect sunlight	The downward scattered irradiation originating from the hemisphere. The light scattering caused commonly by clouds or greenhouse cover (Wald, 2018).
Phenotypic plasticity	Plants' ability to alter its morphology and physiology in response to changes in the environment (Schlichting, 1986).
Photosynthetic capacity	Measure of the maximum carbon fixation rate by photosynthesis expressed in amount of carbon dioxide that is fixed per metre squared per second (μmol m^{-2} s^{-1}) (Hopkins & Hüner, 2009)
Phylloclimate	The physical environment that individual areal plant organs of a plant population experience such as spectral irradiance, temperature, wind speed, and humidity (Chelle, 2005).
Plant architecture	Three-dimensional build-up of the plant body including branching pattern, size, shape and position of the leaves, stems and flowers (Reinhardt & Kuhlemeier, 2002).
Sink strength	The maximum potential organ growth in case the demand for assimilates would be satisfied at all times (Marcelis, 1996).

10.2 Climate measurements

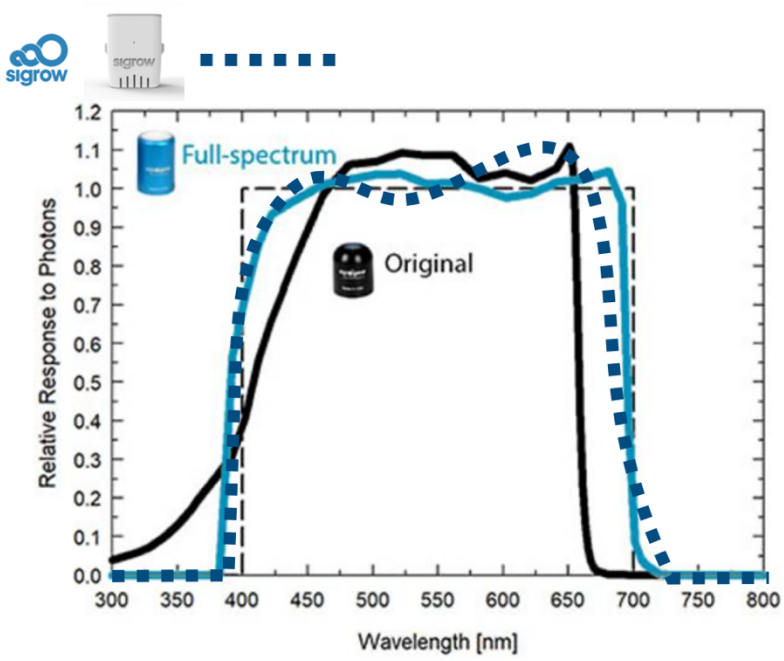

Figure A1. Sigrow and full-spectrum quantum response in photon units.

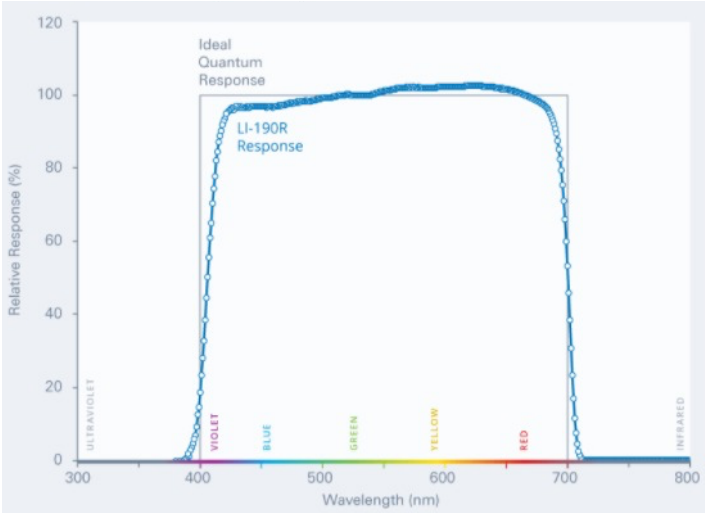

Figure A2. The Li-190R quantum response and the ideal quantum response in photon units.

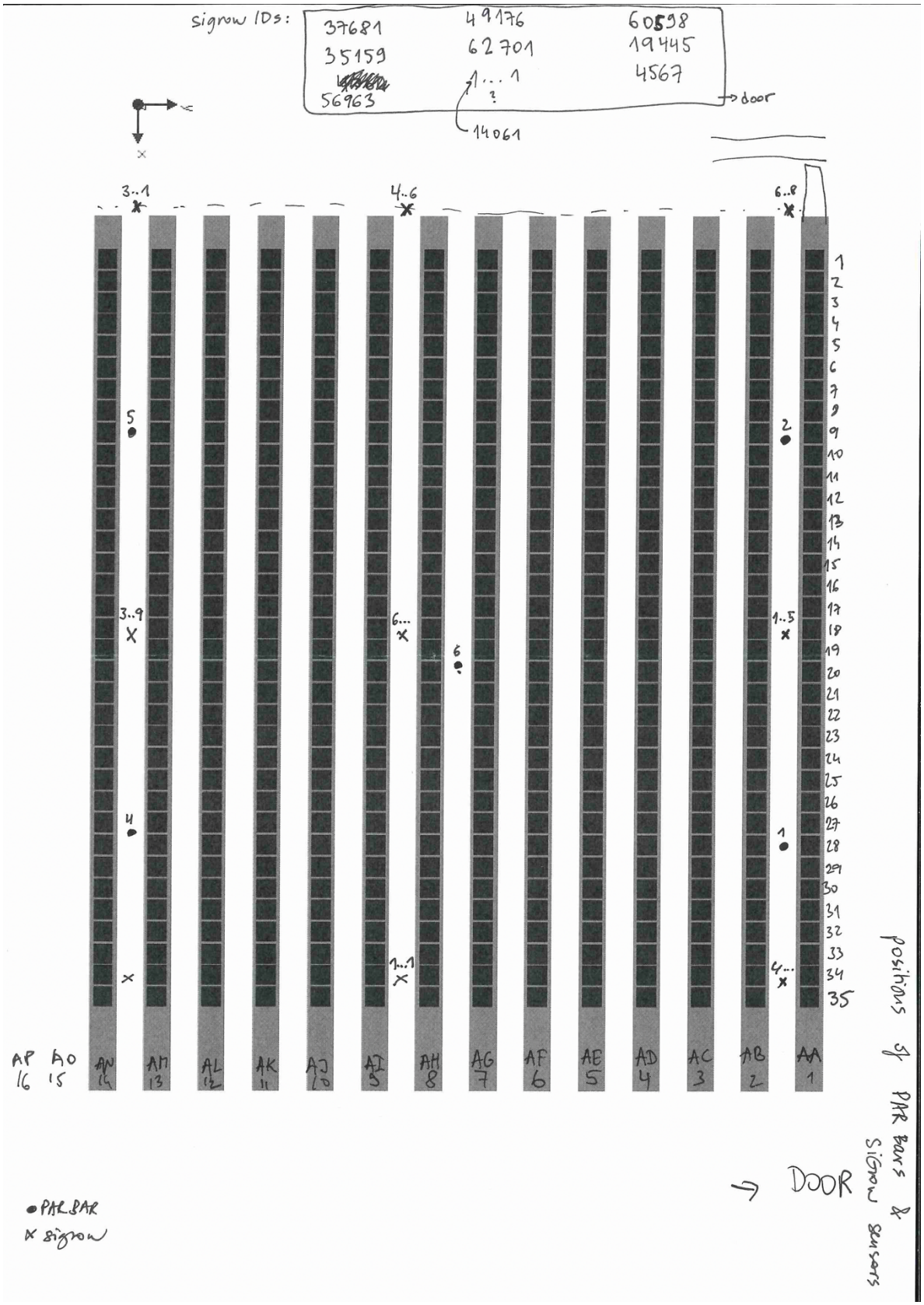

Figure A3. The Sigrow sensor positions within the greenhouse compartment.

10.3 Leaf optical properties

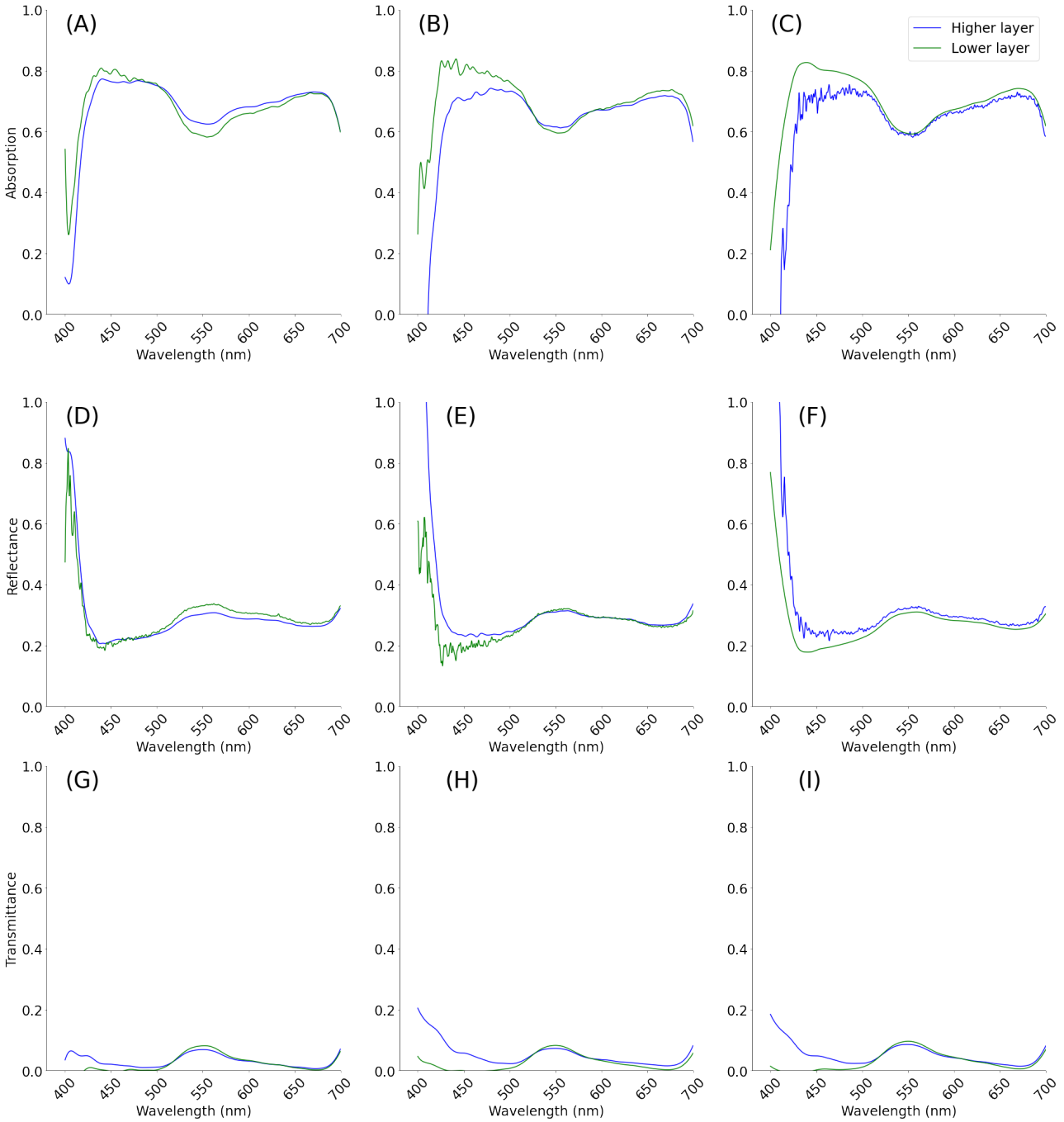

Figure A4. The average abaxial leaf absorption (A, B, C), reflectance (D, E, F) and transmittance (G, H, I) for three tomato varieties (left: Brioso, middle: Merlice, and right: Moneymaker) plotted against the wavelengths for the PAR spectrum (400 – 700 nm) comparing the higher leaf layer (blue) and lower leaf layer (green). The number of replicates can be found in the Appendix A.

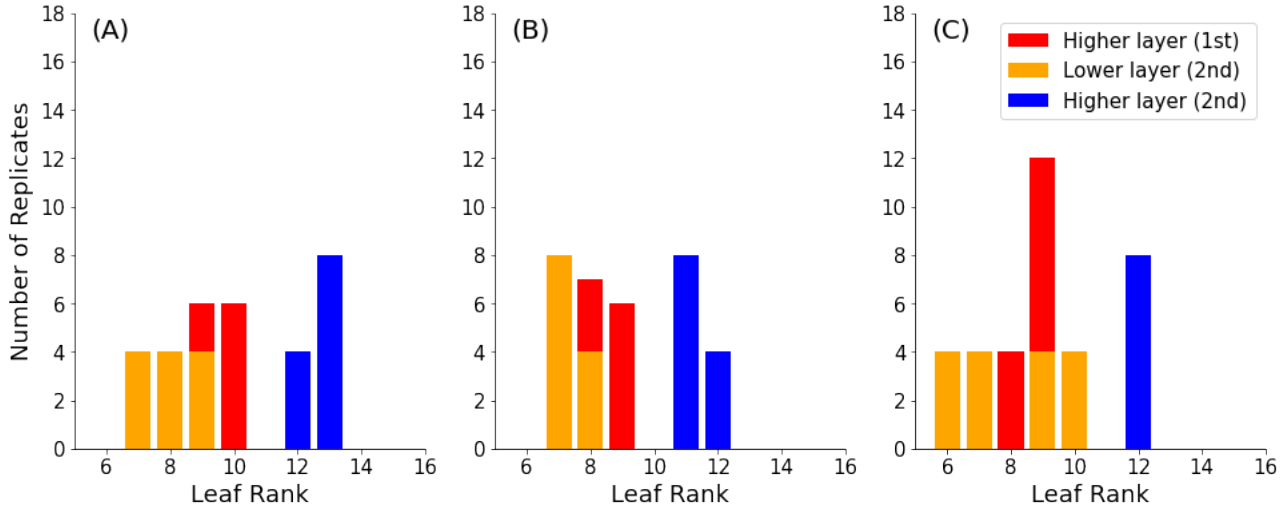

Figure A5. Leaf rank distribution for three tomato varieties (A: Brioso, B: Merlice, and C: Moneymaker) for the leaf optical property measurements divided in the higher layer first day measurements (red) and in the second day measurements containing a higher leaf layer (ranks > 10; blue) and lower leaf layer (ranks ≤ 10; orange).

Table A2. The average leaf absorption of the adaxial and abaxial side for three colours (blue, green, and red) and the full PAR spectrum (450 - 700 nm) for all three tomato varieties (Brioso, Merlice, Moneymaker). Including an ANOVA test (p = 0.05) when comparing the abaxial and abaxial leaf side.

Variety	Colour	Spectrum	Adaxial	Abaxial	p-value
Brioso	Blue	450 - 500 nm	0.80 ± 0.010	0.77 ± 0.012	0.03
	Green	500 - 600 nm	0.72 ± 0.003	0.66 ± 0.004	0.00
	Red	600 - 700 nm	0.75 ± 0.003	0.70 ± 0.004	0.00
	PAR	450 - 700 nm	0.75 ± 0.005	0.70 ± 0.005	0.01
Merlice	Blue	450 - 500 nm	0.78 ± 0.017	0.75 ± 0.017	0.18
	Green	500 - 600 nm	0.71 ± 0.005	0.65 ± 0.005	0.00
	Red	600 - 700 nm	0.74 ± 0.005	0.70 ± 0.005	0.00
	PAR	450 - 700 nm	0.74 ± 0.007	0.69 ± 0.007	0.10
Moneymaker	Blue	450 - 500 nm	0.79 ± 0.015	0.75 ± 0.017	0.06
	Green	500 - 600 nm	0.71 ± 0.005	0.64 ± 0.007	0.00
	Red	600 - 700 nm	0.75 ± 0.005	0.70 ± 0.006	0.00
	PAR	450 - 700 nm	0.74 ± 0.007	0.69 ± 0.008	0.03

10.4 Leaf photosynthesis

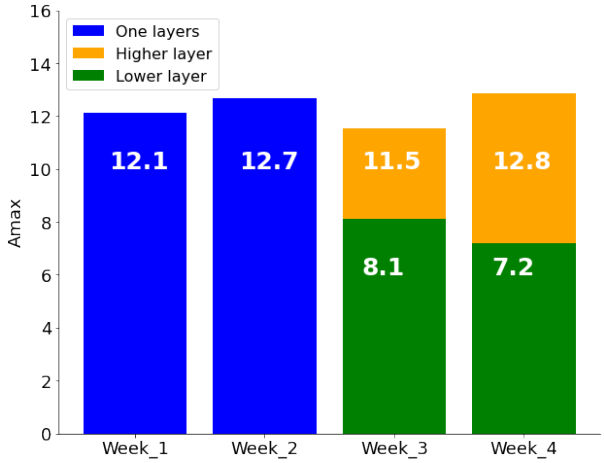

Figure A6. The LRC of the maximum net photosynthesis rate at 2000 µmol m^{-2} s^{-1} for the Merlice variety divided in the first, second, third and fourth week measurements. The first- and second-week measurements were only taken at one layer. The third- and fourth-week measurements were divided in a higher leaf layer (ranks > 10) and lower leaf layer (ranks ≤ 10).

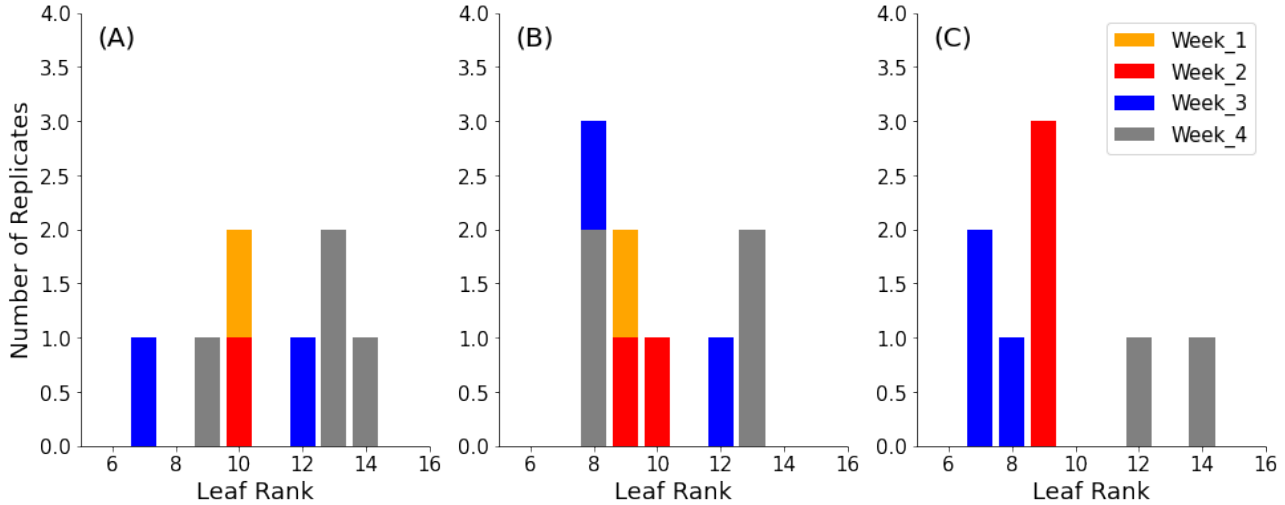

Figure A7. Leaf rank distribution for three tomato varieties (A: Brioso, B: Merlice, and C: Moneymaker) for the LRC and A / Ci photosynthesis measurements divided in the first, second, third and fourth measurement week.

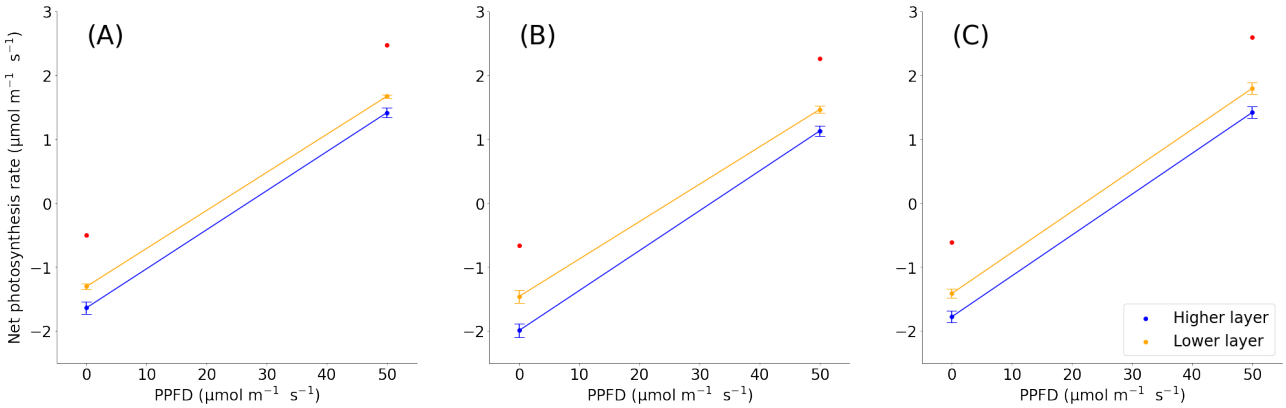

Figure A8. The LRC of the net photosynthesis rate for a range of 0 – 50 µmol m^{-2} s^{-1} (A, B, C) for three tomato varieties (A: Brioso, B: Merlice, C: Moneymaker) divided in a higher leaf layer (blue) and lower leaf layer (orange). During the measurements the Ca was kept at 400 PPM and leaf temperature at 25°C. The error bars indicate the standard error of

means. Red points indicate significant differences between the higher and lower leaf layer at the same PPFD level ($p \leq 0.05$). The number of replicates can be found in the Appendix A.

Table A3. Dark respiration rate (µmol m^{-2} s^{-1}) for Brioso, Merlice, and Moneymaker as determined from the LRC at measurement.

Leaf layer	Brioso	Merlice	Moneymaker
Higher	1.64 ± 0.10 a	2.00 ± 0.11 a	1.78 ± 0.09 a
Lower	1.30 ± 0.04 b	1.46 ± 0.10 b	1.41 ± 0.07 b

10.5 Leaf stomatal conductance

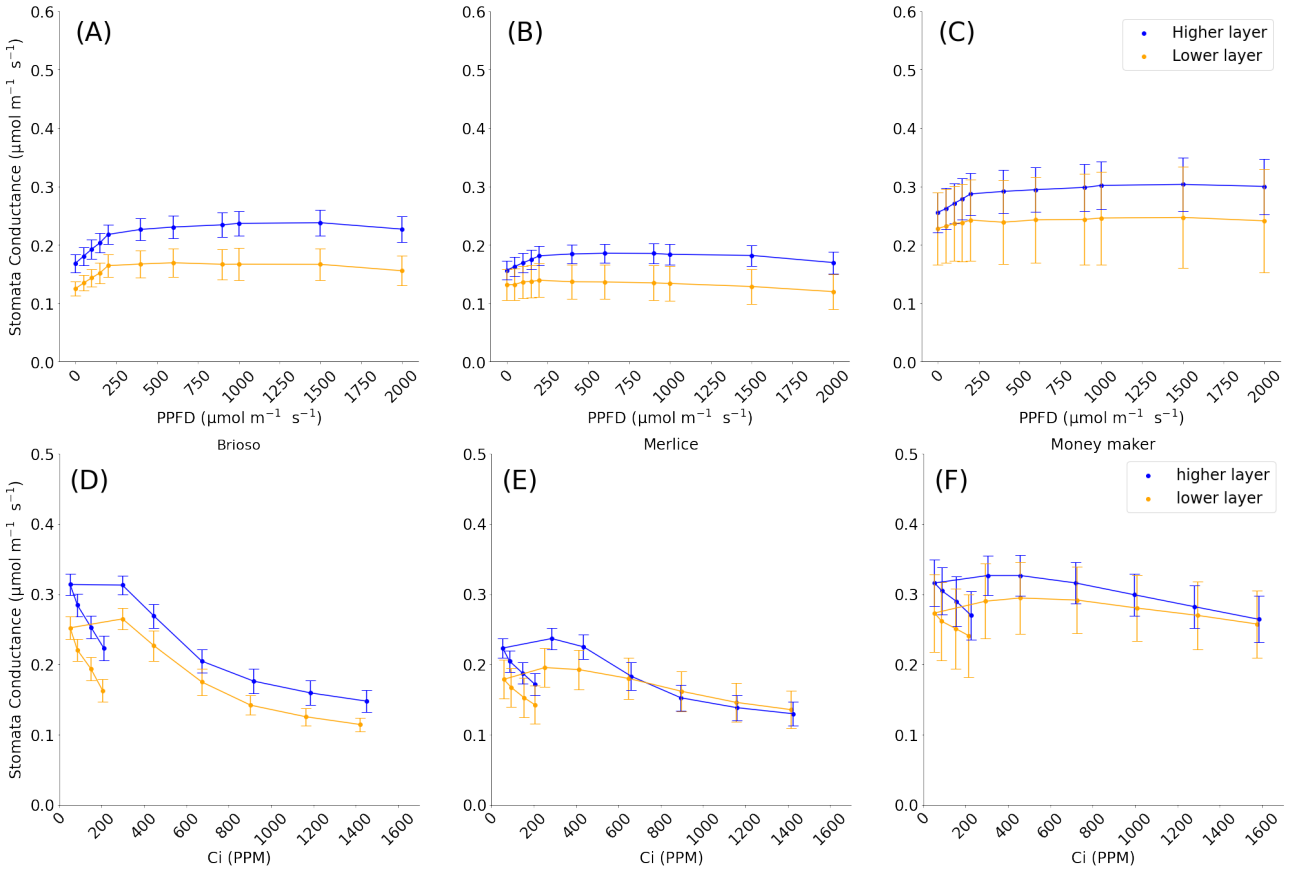

Figure A9. The stomata conductance during the light response curve (A, B, C) and A / Ci curve (C, D, E) for three tomato varieties (Brioso; left, Merlice; middle, Moneymaker; right) divided in a higher leaf layer (ranks > 10) and lower leaf layer (ranks ≤ 10). During the measurements the leaf temperature at 25°C. The error bars indicate the standard error of means. No significant differences were found between the higher and lower layer per variety ($p \leq 0.05$). The number of replicates can be found in the Appendix A.

10.6 Destructive harvest

Table A4. Number of replicates for the destructive harvesting (plant level) from week 1 to 8 per variety (Brioso, Merlice, Moneymaker).

Variety	HW[1] 1	HW 2	HW 3	HW 4	HW 5	HW 6	HW 7	HW 8
Brioso	3	3	6	6	6	6	6	6
Merlice	3	3	6	6	6	6	6	6
Moneymaker	3	3	6	6	6	6	6	6

[1]Harvest Week (HW)

Table A5. Destructive harvesting measurements at plant level.

Plant level	Unit	Description
stem height	cm	stem height from the soil to the beginning of top leaf
number of leaves appeared	-	total number of appeared leaves per plant (leaf counted if >= 5cm long), also those that fell off
number of leaves on plant	-	total number of remaining leaves per plant (leaf counted if >= 5cm long)
number of trusses	-	total number of trusses per plant (not counted if it is above a leaf that is < 5cm)
leaves fresh weight	g	total fresh weight of leaves (including petioles)
Side shoots fresh weight	g	total fresh weight of side shoots
internodes fresh weight	g	total fresh weight of internodes
leaves area	cm2	total leaf area (only if the plant is measured as whole)
cotyledons +small leaves fresh weight	g	total weight of cotyledons + leaves smaller than 5cm
trusses fresh weight	g	total fresh weight of whole trusses (fruits+branching structure)
leaves dry weight	g	total dry weight of leaves (including petioles)
internodes dry weight	g	total dry weight of internodes
trusses dry weight	g	total dry weight of trusses, incl flowers/fruits

Table A6. Destructive harvesting measurements at organ level.

Organ / phytometer level	Unit	Description
rank	-	
internode length	cm	internode length, starting below a leaf up to below the consecutive leaf
internode diameter	mm	internode diameter, at the middle position, measured only at rank 1 and for each internode bearing a truss
internode diameter2	mm	internode diameter, at the middle position, perpendicular to int_diameter2, measured only at rank 1 and for each internode bearing a truss
leaf width	cm	max width of a leaf (maintaining the leaflet/ petiolule angle from rachis; not straighten the leaflets up)
leaf length	cm	leaf length from the stem to the tip of the terminal leaflet
phytometer angle	°	phyllotactic angle of a leaf/truss (clockwise)
branch angle	°	inclination angle of a leaf/truss to the horizontal

number of flowers	-	number of flowers in the truss
number of fruits	-	number of SET fruits in the truss (SET = flower petals pointing backwards (no fruit is visible yet) OR visible fruit)
truss length	cm	length from the stem to the tip of the truss rachis
leaf area	cm^2	area of the leaf (including petiole)
leaf fresh weight	g	leaf fresh weight (including petiole)
Internode fresh weight	g	internode fresh weight
Fruit fresh weight	g	fresh weight of the truss

10.7 GroIMP

Table A7. The optical properties (absorption, reflectance, transmittance) of the adaxial and abaxial leaf side divided in the higher and lower leaf for Merlice.

Layer	Higher		Lower	
Leaf side	Adaxial	Abaxial	Adaxial	Abaxial
Absorption	0.730	0.675	0.735	0.692
Reflectance	0.242	0.295	0.240	0.284
Transmittance	0.028	0.030	0.024	0.025

Table A8. Non-rectangular hyperbola from the Thornley parameter fitting of α (apparent quantum yield), ξ (curve convexity) and A_{sat} (light-saturated photosynthesis rate) the higher leaf layer (ranks >10) and lower leaf layer (ranks ≤ 10) derived from fitting the average LRC of the Merlice.

Layer	α	ξ	A_{sat}
Higher	0.048	0.92	13.57
Lower	0.046	0.92	10.28

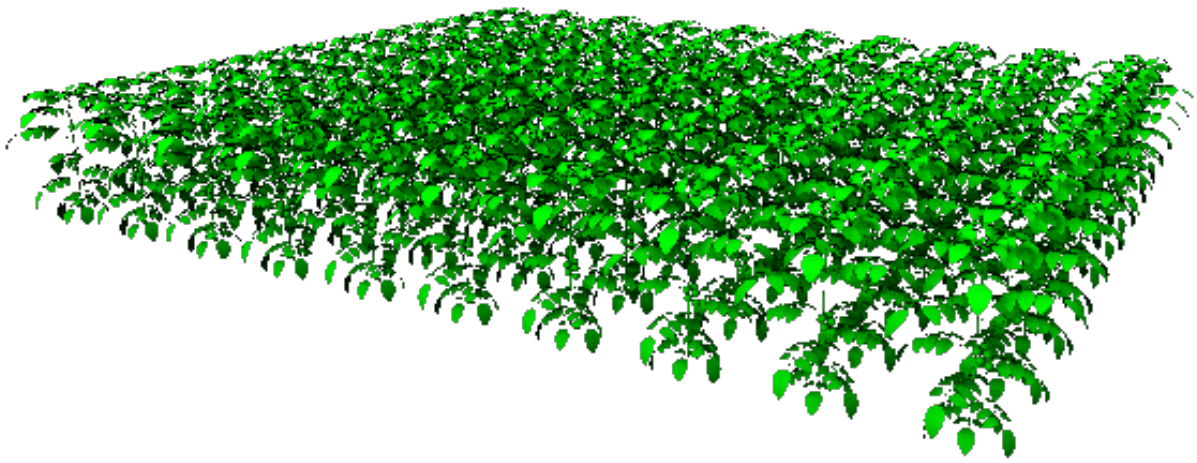

Figure A10. Virtual tomato crop: Simple model

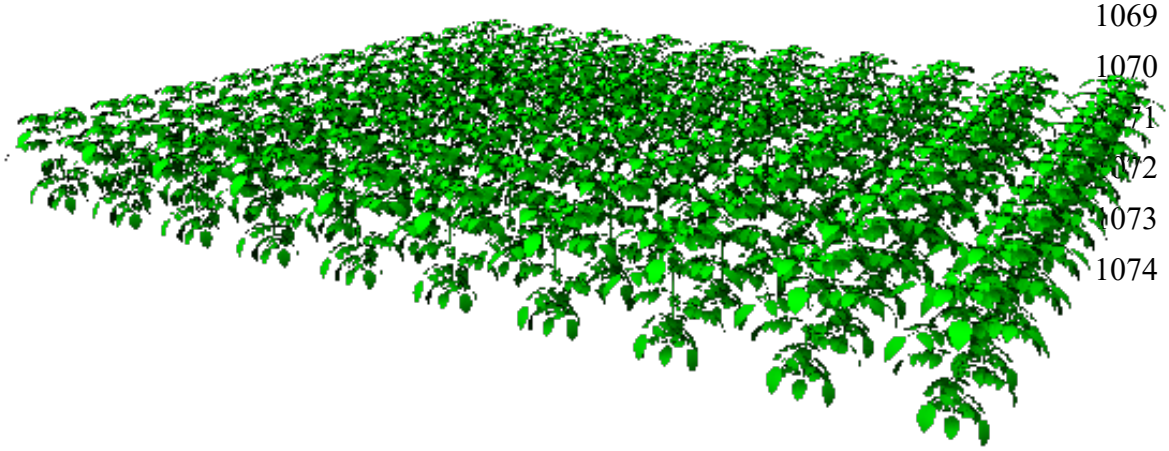

Figure A11. Virtual tomato crop: Complex PS model

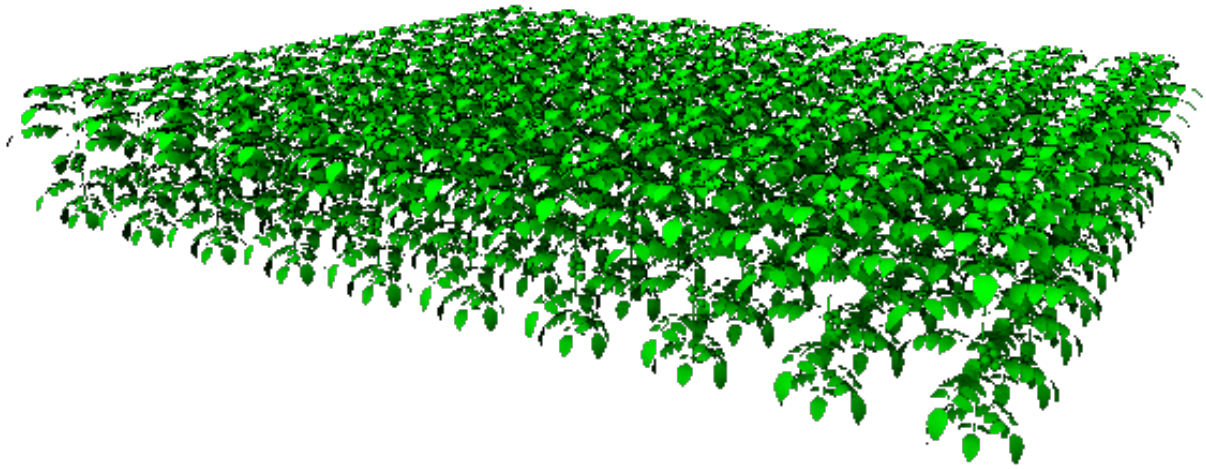

Figure A12. Virtual tomato crop: Complex OP model

10.8 Data storage structuring in MS Teams

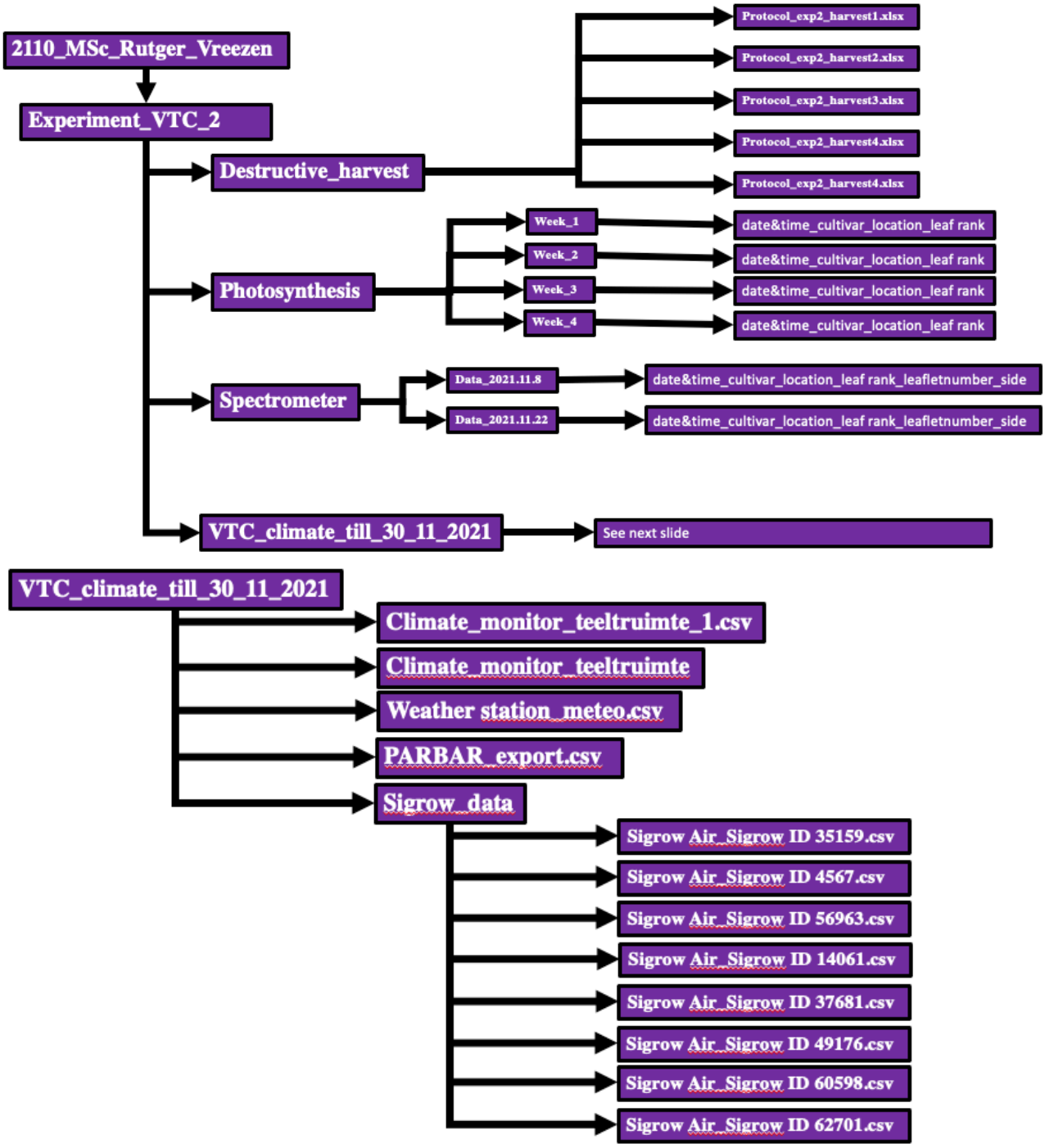

Figure A13. Microsoft teams data organisation.

Appendix B: Statistics

11.1 Python libraries

Table B1. Python libraries used in the data analysis of this research

Library	Purpose (*The Python Standard Library*, 2022)
Pandas	Data manipulation, structuring and analysis.
Numpy	Mathematical operations.
Matplotlib	Data visualization.
Scipy	Provides algorithms tools for optimization, interpolation, statistics, and differential equations.
yaml	Human – readable data-serialization language for file configuration and data storage.
nlopt	Nonlinear optimisation
itertools	Iterator building blocks by standardizing a core set of fast memory tools using iterator algebra.
Math	Provides access to mathematical functions

11.2 Leaf optical properties

Table B2. The average abaxial leaf optical properties for the spectrum waveband of 450 - 700 nm for three tomato varieties (Brioso, Merlice, Moneymaker) when comparing the higher leaf layer and lower leaf layer using an ANOVA test ($p \leq 0.05$).

Variety	OP	Higher	Lower	P - value
Brioso	Absorption	0.701 ± 0.008	0.689 ± 0.003	0.27
	Reflectance	0.270 ± 0.004	0.284 ± 0.003	0.05
	Transmittance	0.029 ± 0.004	0.027 ± 0.001	0.82
Merlice	Absorption	0.684 ± 0.010	0.702 ± 0.005	0.23
	Reflectance	0.277 ± 0.05	0.271 ± 0.004	0.40
	Transmittance	0.039 ± 0.005	0.028 ± 0.004	0.16
Moneymaker	Absorption	0.676 ± 0.011	0.702 ± 0.011	0.13
	Reflectance	0.282 ± 0.006	0.262 ± 0.001	0.09
	Transmittance	0.042 ± 0.005	0.036 ± 0.003	0.39

Table B3. Tukey's HSD to test the significant effect of the factors "Cultivar" including three levels (Brioso, Merlice, Moneymaker) for the leaf absorption.

group1	group2	meandiff	p-adj	lower	upper	reject
brioso	merlice	-0.0092	0.5672	-0.0309	0.0124	FALSE
brioso	moneymaker	-0.0077	0.6525	-0.029	0.0136	FALSE
merlice	moneymaker	0.0015	0.9	-0.0196	0.0226	FALSE

Table B4. Tukey's HSD to test the significant effect of the factors "Cultivar" including three levels (Brioso, Merlice, Moneymaker) for the leaf reflectance.

group1	group2	meandiff	p-adj	lower	upper	reject
brioso	merlice	0.0015	0.9	-0.0155	0.0186	FALSE
brioso	moneymaker	-0.0034	0.8721	-0.0201	0.0134	FALSE
merlice	moneymaker	-0.0049	0.7455	-0.0215	0.0117	FALSE

Table B5. Tukey's HSD to test the significant effect of the factors "Cultivar" including three levels (Brioso, Merlice, Moneymaker) for the leaf transmittance.

group1	group2	meandiff	p-adj	lower	upper	reject
brioso	merlice	0.0077	0.053	-0.0001	0.0155	FALSE
brioso	moneymaker	0.0111	0.0023	0.0034	0.0187	TRUE
merlice	moneymaker	0.0034	0.5413	-0.0042	0.0109	FALSE

Absorption ANOVA test results (Adaxial side side) between higher and lower leaf layer
Brioso: Higher leaf layer x lower leaf layer P - value: 0.5106 = Non-significant
Merlice: Higher leaf layer x lower leaf layer P - value: 0.2041 = Non-significant
Moneymaker: Higher leaf layer x lower leaf layer P - value: 0.17 = Non-significant

Absorption Barlett test results (Adaxial side side) between higher and lower leaf layer
Brioso: BartlettResult(statistic=13.381489055299458, pvalue=0.0002541198975617837)
Merlice: BartlettResult(statistic=11.070808476071484, pvalue=0.0008769743613416805)
Moneymaker: BartlettResult(statistic=5.695958457355598, pvalue=0.017004023730111215)

Absorption Shapiro Wilk test results (Adaxial side side) between higher and lower leaf layer
Higher leaf layer:
Brioso = Statistics 0.83 p-value 0.0193
Merlice = Statistics 0.73 p-value 0.0012
Moneymaker = Statistics 0.82 p-value 0.0148
Lower leaf layer:
Brioso = Statistics 0.94 p-value 0.6639
Merlice = Statistics 0.9 p-value 0.3557
Moneymaker = Statistics 0.94 p-value 0.5969

Reflectance ANOVA test results (Adaxial side side) between higher and lower leaf layer
Brioso: Higher leaf layer x lower leaf layer P - value: 0.2932 = Non-significant
Merlice: Higher leaf layer x lower leaf layer P - value: 0.327 = Non-significant
Moneymaker: Higher leaf layer x lower leaf layer P - value: 0.1061 = Non-significant

Reflectance Barlett test results (Adaxial side side) between higher and lower leaf layer
Brioso: BartlettResult(statistic=12.591202717765233, pvalue=0.0003875666638184438)
Merlice: BartlettResult(statistic=10.78853105326006, pvalue=0.0010213089632650314)
Moneymaker: BartlettResult(statistic=2.62351878654038, pvalue=0.10529071918140501)

Reflectance Shapiro Wilk test results (Adaxial side side) between higher and lower leaf layer
Higher leaf layer:
Brioso = Statistics 0.92 p-value 0.2707
Merlice = Statistics 0.82 p-value 0.0122
Moneymaker = Statistics 0.9 p-value 0.1676
Lower leaf layer:
Brioso = Statistics 0.9 p-value 0.39
Merlice = Statistics 0.98 p-value 0.9611
Moneymaker = Statistics 0.85 p-value 0.1008

Transmittance ANOVA test results (Adaxial side side) between higher and lower leaf layer
Brioso: Higher leaf layer x lower leaf layer P - value: 0.9337 = Non-significant
Merlice: Higher leaf layer x lower leaf layer P - value: 0.1434 = Non-significant
Moneymaker: Higher leaf layer x lower leaf layer P - value: 0.3632 = Non-significant

Transmittance Barlett test results (Adaxial side side) between higher and lower leaf layer
Brioso: BartlettResult(statistic=4.8916941412786805, pvalue=0.02698619303574223)
Merlice: BartlettResult(statistic=1.29673190773446, pvalue=0.2548110422266833)
Moneymaker: BartlettResult(statistic=0.10702410575284935, pvalue=0.7435579231447018)

Transmittance Shapiro Wilk test results (Adaxial side side) between higher and lower leaf layer
Higher leaf layer:
Brioso = Statistics 0.91 p-value 0.2323
Merlice = Statistics 0.91 p-value 0.1906
Moneymaker = Statistics 0.93 p-value 0.334

Lower leaf layer:
Brioso = Statistics 0.93 p-value 0.5507
Merlice = Statistics 0.91 p-value 0.4581
Moneymaker = Statistics 0.89 p-value 0.2272

Absorption ANOVA test results (Abaxial side side) between higher and lower leaf layer
Brioso: Higher leaf layer x lower leaf layer P - value: 0.2718 = Non-significant
Merlice: Higher leaf layer x lower leaf layer P - value: 0.2371 = Non-significant
Moneymaker: Higher leaf layer x lower leaf layer P - value: 0.1276 = Non-significant

Absorption Barlett test results (Abaxial side side) between higher and lower leaf layer:
Brioso: BartlettResult(statistic=7.7511913873552505, pvalue=0.005367711905512713)
Merlice: BartlettResult(statistic=4.417176892405848, pvalue=0.035578854544768855)
Moneymaker: BartlettResult(statistic=0.24685430599755417, pvalue=0.6192988190457828)

Absorption Shapiro Wilk test results (Abaxial side side) between higher and lower leaf layer
Higher leaf layer:
brioso = Statistics 0.83 p-value 0.0193
merlice = Statistics 0.73 p-value 0.0012
moneymaker = Statistics 0.82 p-value 0.0148
Lower leaf layer:
brioso = Statistics 0.95 p-value 0.7246
merlice = Statistics 0.93 p-value 0.5618
moneymaker = Statistics 0.73 p-value 0.0046

Transmittance Barlett test results (Abaxial side side) between higher and lower leaf layer
Brioso: BartlettResult(statistic=6.283380136133995, pvalue=0.012187542283658852)
Merlice: BartlettResult(statistic=0.45183912126935855, pvalue=0.5014628764908805)
Moneymaker: BartlettResult(statistic=3.613245239182348, pvalue=0.05732116249285957)

Transmittance Shapiro Wilk test results (Abaxial side side) between higher and lower leaf layer
Higher leaf layer:
Brioso = Statistics 0.87 p-value 0.0612
Merlice = Statistics 0.91 p-value 0.1863
Moneymaker = Statistics 0.94 p-value 0.5584
Lower leaf layer:
Brioso = Statistics 0.8 p-value 0.0605
Merlice = Statistics 0.88 p-value 0.2573
Moneymaker = Statistics 0.86 p-value 0.1282

Reflectance ANOVA test results (Abaxial side side) between higher and lower leaf layer
Brioso: Higher leaf layer x lower leaf layer P - value: 0.047 = Significant
Merlice: Higher leaf layer x lower leaf layer P - value: 0.4033 = Non-significant
Moneymaker: Higher leaf layer x lower leaf layer P - value: 0.0934 = Non-significant

Reflectance Barlett test results (Abaxial side side) between higher and lower leaf layer
Brioso: Bartlett Result(statistic=3.0012115420085177, pvalue=0.0832022764861368)
Merlice: Bartlett Result(statistic=2.2830925279895253, pvalue=0.13079085133405247)
Moneymaker: Bartlett Result(statistic=0.4407214491492382, pvalue=0.5067744479943812)

Reflectance Shapiro Wilk test results (Abaxial side side) between higher and lower leaf layer
Higher leaf layer:
Brioso = Statistics 0.93 p-value 0.3737
Merlice = Statistics 0.85 p-value 0.0322
Moneymaker = Statistics 0.85 p-value 0.0404

Lower leaf layer:
Brioso = Statistics 0.9 p-value 0.39
Merlice = Statistics 0.98 p-value 0.9611
Moneymaker = Statistics 0.85 p-value 0.1008

Transmittance ANOVA test results (Abaxial side side) between higher and lower leaf layer
Brioso: Higher leaf layer x lower leaf layer P - value: 0.8209 = Non-significant
Merlice: Higher leaf layer x lower leaf layer P - value: 0.1631 = Non-significant
Moneymaker: Higher leaf layer x lower leaf layer P - value: 0.3936 = Non-significant

Transmittance Barlett test results (Abaxial side side) between higher and lower leaf layer
Brioso: BartlettResult(statistic=8.566784494046471, pvalue=0.003423512534342816)
Merlice: BartlettResult(statistic=1.9197971302840966, pvalue=0.16587902629905243)
Moneymaker: BartlettResult(statistic=4.536342069351669, pvalue=0.033182427938176544)

11.3 Leaf photosynthesis

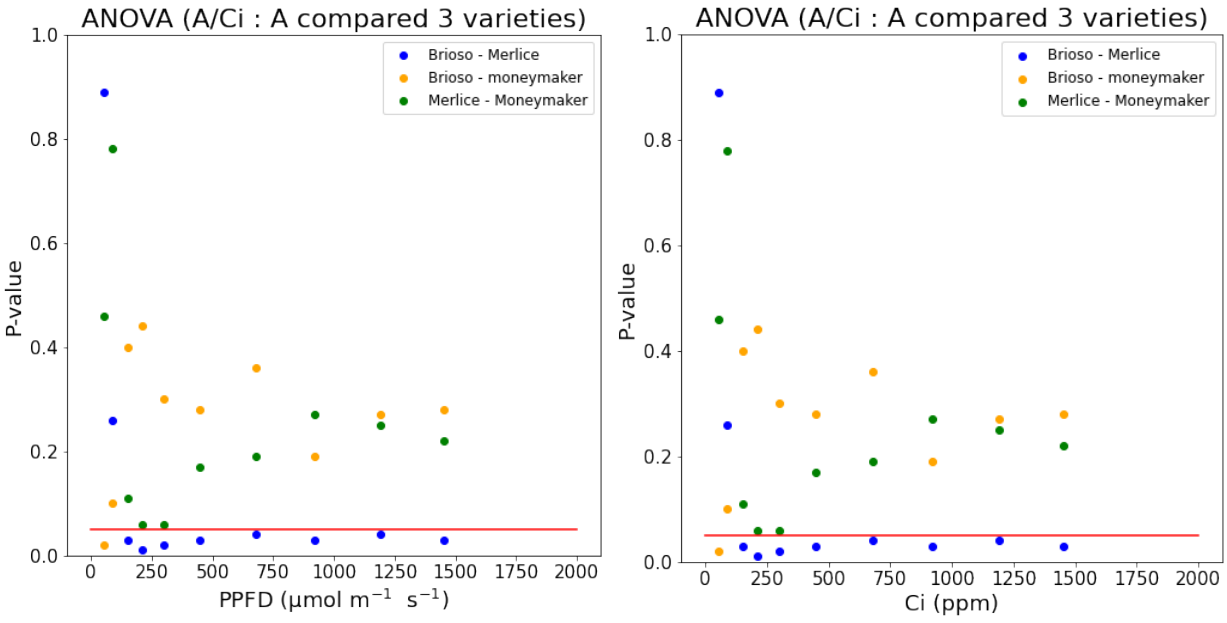

Figure B1. The LRC and A / Ci curve ANOVA results of the net photosynthesis rate compared for three tomato varieties (blue: Brioso - Merlice, orange: Brioso - Moneymaker, green: Merlice - Moneymaker). During the measurements the leaf

temperature was kept at 25°C. The error bars indicate the standard error of means. The points below 0.05 indicate that the varieties' net photosynthesis rate was significantly different ($p \leq 0.05$) compared to the other varieties at the same level of PPFD or Ci . The number of replicates can be found in the Appendix A.

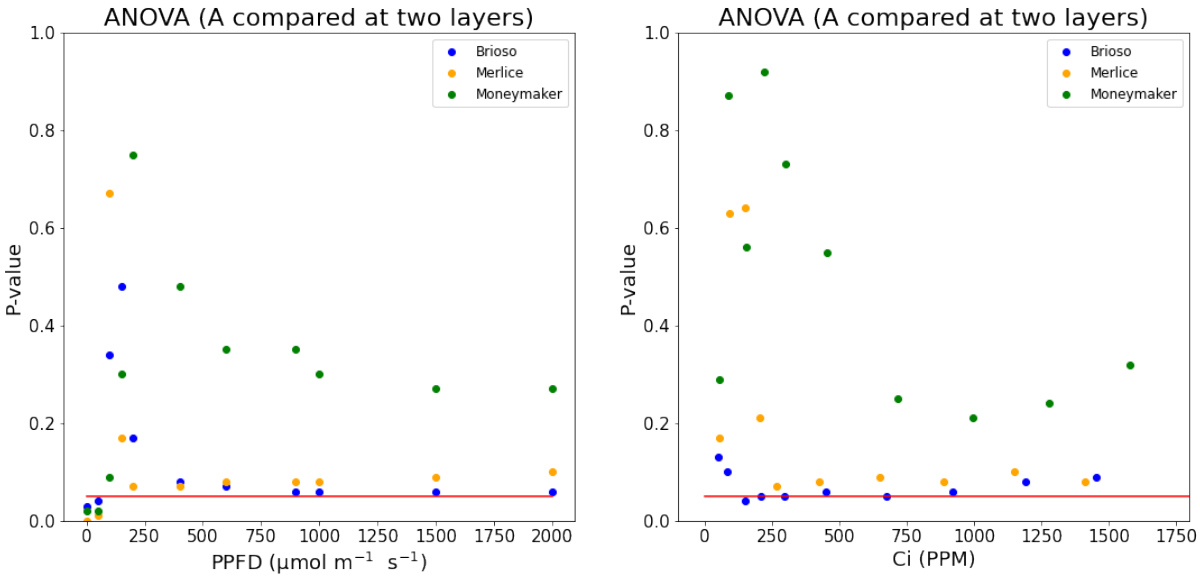

Figure B2. The ANOVA results of the net photosynthesis rate of the LRC and A/Ci curve of the higher and lower leaf layer for the three tomato varieties (blue: Brioso, orange: Merlice, green: Moneymaker). Points below 0.05 indicate significant differences between the higher and lower leaf layer at identical PPFD level or ppm ($p \leq 0.05$). The number of replicates can be found in the Appendix A.

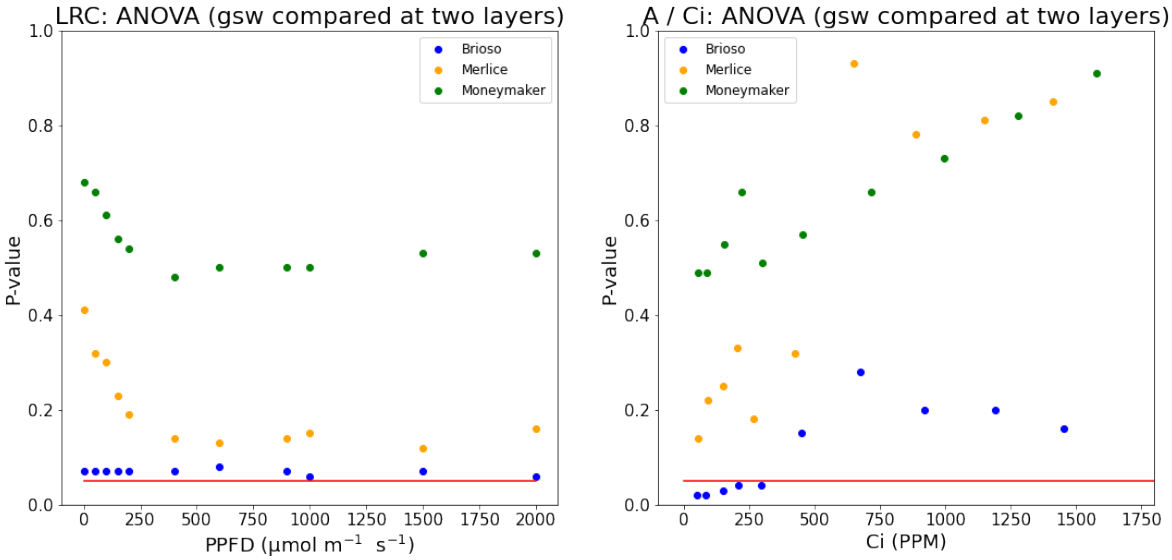

Figure B3. The ANOVA results of the stomata conductance of the LRC and A/Ci curve of the higher and lower leaf layer for the three tomato varieties (blue: Brioso, orange: Merlice, green: Moneymaker). Points below 0.05 indicate significant differences between the higher and lower leaf layer at identical PPFD level or ppm ($p \leq 0.05$). The number of replicates can be found in the Appendix A.

11.4 Destructive harvest

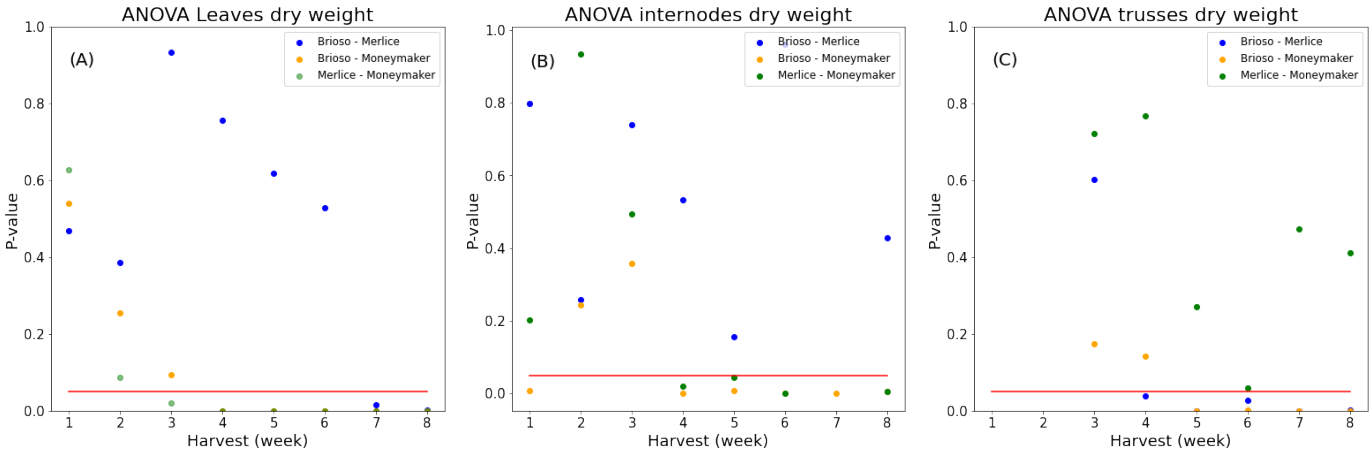

Figure B4. The ANOVA test for all harvest weeks (1 – 8) for the response variables leaves (A) stem (B) and trusses (C) for three tomato varieties (Brioso, Merlice, and Moneymaker). Points below the red line indicate that the organ dry weight of the variety was significantly different from organ dry weight of the other variety within the same week ($p \leq 0.05$).

Table B6 . Tukey's HSD to test the significant effect of the factors "Cultivar" including three levels (Brioso, Merlice, Moneymaker) for the dry stem weight of the 6th harvest.

group1	group2	meandiff	p-adj	lower	upper	reject
Brioso	Merlice	0.0383	0.9	-1.7779	1.8546	False
Brioso	Moneymaker	-4.14	0.001	-5.9563	-2.3237	True
Merlice	Moneymaker	-4.1783	0.001	-5.9946	-2.3621	True

Table B7. Tukey's HSD to test the significant effect of the factors "Cultivar" including three levels (Brioso, Merlice, Moneymaker) for the dry leaves weight of the 6th harvest.

group1	group2	meandiff	p-adj	lower	upper	reject
Brioso	Merlice	1.2333	0.747	-3.2643	5.731	False
Brioso	Moneymaker	-15.5017	0.001	-19.9993	-11.004	True
Merlice	Moneymaker	-16.735	0.001	-21.2327	-12.2373	True

Table B8. Tukey's HSD to test the significant effect of the factors "Cultivar" including three levels (Brioso, Merlice, Moneymaker) for the dry trusses weight of the 6th harvest.

group1	group2	meandiff	p-adj	lower	upper	reject
Brioso	Merlice	-2.7367	0.0343	-5.2799	-0.1935	True
Brioso	Moneymaker	-4.5783	0.001	-7.1215	-2.0351	True
Merlice	Moneymaker	-1.8417	0.1784	-4.3849	0.7015	False

Table B9. Tukey's HSD to test the significant effect of the factors "Cultivar" including three levels (Brioso, Merlice, Moneymaker) for the stem partitioning of the 6th harvest.

group1	group2	meandiff	p-adj	lower	upper	reject
Brioso	Merlice	0.735	0.7271	-1.8188	3.2889	False
Brioso	Moneymaker	4.9488	0.001	2.395	7.5027	True
Merlice	Moneymaker	4.2138	0.0018	1.6599	6.7677	True

Table B10. Tukey's HSD to test the significant effect of the factors "Cultivar" including three levels (Brioso, Merlice, Moneymaker) for the leaves partitioning of the 6th harvest.

group1	group2	meandiff	p-adj	lower	upper	reject
Brioso	Merlice	3.4987	0.1783	-1.3312	8.3286	False
Brioso	Moneymaker	-2.5325	0.386	-7.3625	2.2974	False
Merlice	Moneymaker	-6.0312	0.0142	-10.8611	-1.2013	True

Table B11. Tukey's HSD to test the significant effect of the factors "Cultivar" including three levels (Brioso, Merlice, Moneymaker) for the trusses partitioning of the 6th harvest.

group1	group2	meandiff	p-adj	lower	upper	reject
Brioso	Merlice	0.735	0.7271	-1.8188	3.2889	False
Brioso	Moneymaker	4.9488	0.001	2.395	7.5027	True
Merlice	Moneymaker	4.2138	0.0018	1.6599	6.7677	True

Shapiro test results for Brioso of the 6th harvest.
Brioso & leaves_dw = Shapiro test 0.82 p-value 0.0966
Brioso & internodes_dw = Shapiro test 0.9 p-value 0.3843
Brioso & trusses_dw = Shapiro test 0.86 p-value 0.1782
Brioso & relative_leaves = Shapiro test 0.76 p-value 0.0256
Brioso & relative_trusses = Shapiro test 0.79 p-value 0.0481
Brioso & relative_internodes = Shapiro test 0.93 p-value 0.5797

Shapiro test results for Merlice of the 6th harvest.
Merlice & leaves_dw = Shapiro test 0.87 p-value 0.2326
Merlice & internodes_dw = Shapiro test 0.9 p-value 0.3804
Merlice & trusses_dw = Shapiro test 0.8 p-value 0.0603
Merlice & relative_leaves = Shapiro test 0.96 p-value 0.8476
Merlice & relative_trusses = Shapiro test 0.89 p-value 0.301
Merlice & relative_internodes = Shapiro test 0.92 p-value 0.5257

Shapiro test results for Moneymaker of the 6th harvest.
Merlice & leaves_dw = Shapiro test 0.87 p-value 0.2326
Merlice & internodes_dw = Shapiro test 0.9 p-value 0.3804
Merlice & trusses_dw = Shapiro test 0.8 p-value 0.0603
Merlice & relative_leaves = Shapiro test 0.96 p-value 0.8476
Merlice & relative_trusses = Shapiro test 0.89 p-value 0.301
Merlice & relative_internodes = Shapiro test 0.92 p-value 0.5257

Bartlett test results for all three tomato varieties of the 6th harvest.
internodes_dw = Bartlett test 0.3 p-value 0.8614
leaves_dw = Bartlett test 1.41 p-value 0.4934
trusses_dw = Bartlett test 5.29 p-value 0.0711
relative_leaves = Bartlett test 3.15 p-value 0.207
relative_trusses = Bartlett test 1.06 p-value 0.5897
relative_internodes = Bartlett test 7.24 p-value 0.0267